Upwind-Difference Potentials Method for Patlak-Keller-Segel Chemotaxis Model

Yekaterina Epshteyn[1]

Abstract

We develop a novel upwind-difference potentials method for the Patlak-Keller-Segel chemotaxis model that can be used to approximate problems in complex geometries. The chemotaxis model under consideration is described by a system of two nonlinear PDEs: a convection-diffusion equation for the cell density coupled with a reaction-diffusion equation for the chemoattractant concentration.

Chemotaxis is an important process in many medical and biological applications, including bacteria/cell aggregation and pattern formation mechanisms, as well as tumor growth. Furthermore modeling of real biomedical problems often has to deal with the complex structure of computational domains. There is consequently a need for accurate, fast, and computationally efficient numerical methods for different chemotaxis models that can handle arbitrary geometries.

The upwind-difference potentials method proposed here handles complex domains with the use of only Cartesian meshes, and can be easily combined with fast Poisson solvers. In the numerical tests presented below we demonstrate the robustness of the proposed scheme.

AMS subject classification: 65M06, 65M08, 65M22, 65M70, 92C17, 35K57

Key words: Patlak-Keller-Segel chemotaxis model, convection-diffusion-reaction systems, finite difference, finite volume, Difference Potentials methods, Cartesian meshes, complex domains.

1 Introduction

In this work we develop a novel upwind-difference potentials method for the chemotaxis models and closely related problems in physics and biology that can handle complex geometries without the use of unstructured meshes. We consider the most common formulation of the classical Patlak-Keller-Segel system [12] with the 'parabolic-parabolic' coupling, which can be written in the dimensionless form as

$$\begin{cases} \rho_t + \nabla\cdot(\chi\rho\nabla c) = \Delta\rho, \\ c_t = \Delta c - c + \rho, \end{cases} \qquad (x,y)\in\Omega, t>0, \tag{1.1}$$

subject to the Neumann boundary conditions:

$$\nabla\rho\cdot\mathbf{n} = \nabla c\cdot\mathbf{n} = 0, \quad (x,y)\in\partial\Omega. \tag{1.2}$$

Here, $\rho(x,y,t)$ is the cell density, $c(x,y,t)$ is the chemoattractant concentration, χ is a chemotactic sensitivity constant, Ω is a bounded domain in $\mathbb{R}^2$, $\partial\Omega$ is its boundary, and $\mathbf{n}$ is a unit normal vector.

Chemotaxis refers to mechanisms by which cellular motion occurs in response to an external stimulus, usually a chemical one. Chemotaxis is an important process in many medical and biological applications, including bacteria/cell aggregation and pattern formation mechanisms, as well as tumor growth. There exists an extensive literature about chemotaxis models and their mathematical analysis. A first place to start is [37], as well as [24, 25], and for a deeper background [2, 14, 34, 1, 12, 4, 5, 38]. The first descriptions of the mechanism owe to Keller and Segel, [27, 28, 29] and Patlak [36]. In this description, the organism or migrating enzyme chooses a direction upwards of a chemical signal which leads to aggregation.

---

[*] Department of Mathematics, The University of Utah, Salt Lake City, UT, 84112, `epshteyn@math.utah.edu`

Although there is an extensive literature on this subject, only a few numerical methods have been proposed for these models. Chemotaxis models are usually highly nonlinear due to the density dependent cross diffusion term (attracting force) that models chemotactic behavior, and hence, any realistic chemotaxis model is too difficult to solve analytically. Therefore, development of accurate and efficient numerical methods is crucial for the modeling and analysis of chemotaxis systems. Furthermore, a common property of all existing chemotaxis systems is their ability to model a concentration phenomenon that mathematically results in rapid growth of solutions in small neighborhoods of concentration points/curves. The solutions may blow up or may exhibit a very singular, spiky behavior. This blow-up represents a mathematical description of a cell concentration phenomenon that occurs in real biological systems, see, e.g., [1, 2, 4, 5, 14, 38]. In either case, capturing such solutions numerically is a very challenging problem.

Let us briefly review the numerical methods that have been proposed in the literature. A finite-volume, [21], and finite-element, [32, 41], methods have been proposed for a simplified version of the Patlak-Keller-Segel model with 'parabolic-elliptic' coupling: the equation for concentration of chemical signals c has been replaced by an elliptic equation using an assumption that c changes over much smaller time scales than the density of the cells ρ. A fractional step numerical method for a fully time-dependent chemotaxis system from [44] has been proposed in [45]. However, the operator splitting approach may not be applicable when a convective part of the chemotaxis system is not hyperbolic, which is a generic situation for the original Patlak-Keller-Segel model with 'parabolic-parabolic' coupling. In [11], a second order finite-volume central-upwind scheme was derived for the original Patlak-Keller-Segel model and extended to some other chemotaxis models. Recently, in [42], an implicit flux-corrected finite element method has been developed for the original Patlak-Keller-Segel model as well. In our work [20, 19, 18] we developed a family of high-order finite element methods for the original Patlak-Keller-Segel chemotaxis model (discontinuous Galerkin method) which was designed to handle rectangular domains. However, in spite of several advantages (see for example [20]), some known drawbacks with the discontinuous Galerkin schemes are their high memory and computational costs and very involved implementation compare to continuous Galerkin finite element, finite volume, or finite difference methods. Also, let us note that among the methods that have been proposed, only [32, 41, 42] were designed to treat complex geometry and only by the use of unstructured meshes. In general, the design of such methods on unstructured meshes is a more challenging task and these methods are usually more computationally intensive since development of slope limiters techniques, insurance of the positivity preserving property as well as proper approximation of the diffusive fluxes (in order to guarantee the desired stability property of the numerical scheme) becomes a rather difficult question on unstructured meshes (see for example some recent work [6, 7, 13, 3, 42, 16, 15, 17]) compared to the design of such methods on Cartesian grids (see for example [35, 31, 33, 8, 11, 30]). Finally, a different approach has been proposed in [22]. The authors considered the measure-valued global in time solutions of the simplified Patlak-Keller-Segel system in $\mathbb{R}^2$ and proposed a stochastic particle approximation. The advantage of their method is that it captures the solution even after the (possible) blow-up. However, the method was only designed for the simplified Patlak-Keller-Segel model with 'parabolic-elliptic' coupling. Moreover, at least in the 2D case, methods based on particle simulation are usually less efficient than 'conventional' finite element or finite volume methods for solving convection-diffusion equations.

Often, modeling of real biomedical problems has to deal with the complex structure of the computational domains. Therefore there is a need for accurate, fast, and computationally efficient numerical methods for different chemotaxis models that can handle arbitrary geometries.

In this paper we develop novel and efficient upwind-difference potentials method which can handle complex geometry without the use of unstructured meshes (with the consideration of only Cartesian grids) and that can be employed with fast Poisson solvers. Our method combines the simplicity of positivity-preserving upwind scheme for chemotaxis models on Cartesian meshes [10] with the flexibility of the Difference Potentials method [40].

The paper is organized as follows. First, in Section 1.1 we give a brief summary of the main steps of the proposed algorithm. Then, we make an overview of the positivity-preserving upwind scheme for chemotaxis models on Cartesian meshes in Section 1.2, and an overview of the Difference Potentials Method (DPM) in Section 1.3. In Section 1.4 we described the approximation of the boundary conditions. For the readers convenience we present the proofs of some results for the upwind-difference potentials method applied to the chemotaxis model under consideration in Appendix Section 3. Finally, we illustrate the performance of the proposed scheme in several numerical experiments in Section 2. Some concluding remarks are given in Section 4.

1.1 Algorithm

In this section we will briefly summarize the steps of our algorithm. In the subsequent sections below we will give the detailed description of each step.

- *Step 1:* First, at each time level t^{i+1} we compute *auxiliary solution* $\mathbf{f} = (f^{\bar{\rho}}, f^{c})$, (1.15) using a positivity preserving upwind scheme on Cartesian mesh as the solution of the *Auxiliary Problem* (1.11)-(1.14), with the right hand-sides defined in (1.16)-(1.17) (the detailed description is given in Sections 1.2 and 1.3).

- *Step 2:* Next, we compute *boundary values* on γ - $\bar{\rho}^{\gamma}$ and c^{γ} (value of the unknown density $\mathbf{v}_{\gamma}$ on γ) by solving the system of linear equations which is derived from the system of boundary equations (1.29)-(1.30) with the use of finite difference approximations (1.31)-(1.32) of the zero Neumann boundary conditions, for example, as in case of the simple geometry; or by considering spectral approximations of the boundary conditions (1.48)-(1.49), for example as in the case of the complex geometry (see Section 1.4 for the detailed description).

- *Step 3:* Using the definition of the difference potential (see Section 1.3) we construct the *Difference Potential* $\mathbf{P}\mathbf{v}_{\gamma} = (u_{\bar{\rho}}, u_c)$ with the density $\mathbf{v}_{\gamma} = (\bar{\rho}^{\gamma}, c^{\gamma})$ obtained from the previous step *Step 2*.

- *Step 4:* Finally, at each time level t^{i+1} *solution* of the discrete Patlak-Keller-Segel problem (1.4) subject to zero Neumann boundary conditions is given as

  $$\mathbf{u}^{\mathbf{pks}} := \mathbf{P}\mathbf{v}_{\gamma} + \mathbf{f}. \tag{1.3}$$

  This conclusion follows from the statement and the proof of Theorem 1.2 (see also problem (1.24) after Theorem 1.2) in Section 1.3.

1.2 Positivity Preserving Upwind Scheme on Cartesian Mesh - An Overview

In this section, we will recall and will formulate the second-order positivity preserving upwind scheme on Cartesian meshes which was proposed for the system (1.1) in a square domain in [10]. We assume here that we consider the Patlak-Keller-Segel system (1.1) in a square domain $D \subset \mathbb{R}^2$. Let us introduce a Cartesian mesh for domain D consisting of the uniform cells $D_{j,k} := [x_{j-\frac{1}{2}}, x_{j+\frac{1}{2}}]\times$

$[y_{k-\frac{1}{2}}, y_{k+\frac{1}{2}}]$ of the size $\Delta x\Delta y$ centered at the point $(x_j := j\Delta x, y_k := k\Delta y)$. Let us also define a five-point stencil $N_{j,k}$ with center placed at (x_j, y_k) to be the set of the following points: $N_{j,k} := \{(x_j, y_k), (x_{j\pm1}, y_k), (x_j, y_{k\pm1})\}$.

We can now state the fully discrete positivity preserving upwind scheme for the Patlak-Keller-Segel system (1.1) similar to our scheme developed on Cartesian grids in [10]:

$$\left\{\begin{array}{ll} \Delta_{j,k}\bar{\rho}^{i+1} - m\bar{\rho}^{i+1}_{j,k} = g^{\rho}_{j,k}, & (x_j, y_k) \in M, \\ \Delta_{j,k}c^{i+1} - mc^{i+1}_{j,k} = g^{c}_{j,k}, & (x_j, y_k) \in M, \end{array}\right. \tag{1.4}$$

where the unknowns for which we will be solving at the time level t^{i+1} are $(\bar{\rho}^{i+1}, c^{i+1})$.
The computed quantities are the cell averages of the density ρ, $\bar{\rho}_{j,k}(t) \approx \frac{1}{\Delta x\Delta y}\int\int_{D^0_{j,k}} \rho(x, y, t)\Delta x\Delta y$ and the point values $c_{j,k}(t) \approx c(x_j, y_k, t)$. Here, we denote $\bar{\rho}^i_{j,k}$ is the computed $\bar{\rho}_{j,k}(t^i)$ at the discrete time level $t^i := i\Delta t$ with time step Δt and $c^i_{j,k}$ is the computed $c_{j,k}(t^i)$.

$\Delta_{j,k}$ denotes the discrete Laplacian obtained using second order central difference formulas for the x and y variables and $m := \frac{1}{\Delta t}$.
The right-hand side for the density equation is evaluated at the previous time level t^i and will be denoted by $g^{\rho}_{j,k}$ for the brevity of the exposition:

$$g^{\rho}_{j,k} := -m\bar{\rho}^i_{j,k} + \frac{H^x_{j+\frac{1}{2},k} - H^x_{j-\frac{1}{2},k}}{\Delta x} + \frac{H^y_{j,k+\frac{1}{2}} - H^y_{j,k-\frac{1}{2}}}{\Delta y}. \tag{1.5}$$

Here,

$$H^x_{j+\frac{1}{2},k} = \chi\rho^i_{j+\frac{1}{2},k}\Big(\frac{c^i_{j+1,k} - c^i_{j,k}}{\Delta x}\Big), \quad H^y_{j,k+\frac{1}{2}} = \chi\rho^i_{j,k+\frac{1}{2}}\Big(\frac{c^i_{j,k+1} - c^i_{j,k}}{\Delta y}\Big) \tag{1.6}$$

are the upwind numerical fluxes with

$$\rho^i_{j+\frac{1}{2},k} = \left\{\begin{array}{l} \widetilde{\rho}^i(x_{j+\frac{1}{2}} - 0, y_k) \text{ if } \Big(\frac{c^i_{j+1,k} - c^i_{j,k}}{\Delta x}\Big) > 0, \\ \widetilde{\rho}^i(x_{j+\frac{1}{2}} + 0, y_k), \text{ otherwise} \end{array}\right.$$

Similarly,

$$\rho^i_{j,k+\frac{1}{2}} = \left\{\begin{array}{l} \widetilde{\rho}^i(x_j, y_{k+\frac{1}{2}} - 0) \text{ if } \Big(\frac{c^i_{j,k+1} - c^i_{j,k}}{\Delta y}\Big) > 0, \\ \widetilde{\rho}^i(x_j, y_{k+\frac{1}{2}} + 0), \text{ otherwise} \end{array}\right.$$

Here,

$$\widetilde{\rho}^i(x, y) = \bar{\rho}^i_{j,k} + (\rho^i_x)_{j,k}(x - x_j) + (\rho^i_y)_{j,k}(y - y_k), \quad (x, y) \in D^0_{j,k} \tag{1.7}$$

is the piecewise linear reconstruction with the slopes $(\rho^i_x)_{j,k}$ and $(\rho^i_y)_{j,k}$ calculated using the minmod limiter,

$$(\rho^i_x)_{j,k} = minmod\Big(2\frac{\bar{\rho}^i_{j+1,k} - \bar{\rho}^i_{j,k}}{\Delta x}, \frac{\bar{\rho}^i_{j+1,k} - \bar{\rho}^i_{j-1,k}}{2\Delta x}, 2\frac{\bar{\rho}^i_{j,k} - \bar{\rho}^i_{j-1,k}}{\Delta x}\Big)$$

and

$$(\rho^i_y)_{j,k} = minmod\Big(2\frac{\bar{\rho}^i_{j,k+1} - \bar{\rho}^i_{j,k}}{\Delta y}, \frac{\bar{\rho}^i_{j,k+1} - \bar{\rho}^i_{j,k-1}}{2\Delta y}, 2\frac{\bar{\rho}^i_{j,k} - \bar{\rho}^i_{j,k-1}}{\Delta y}\Big).$$

The minmod function is defined by

$$minmod(z_1, z_2, ..., z_p) := \left\{\begin{array}{l} min(z_1, z_2, ..., z_p), \text{ if } z_i > 0 \quad \forall i = 1, ..., p, \\ max(z_1, z_2, ..., z_p), \text{ if } z_i < 0 \quad \forall i = 1, ..., p, \\ 0, \text{ otherwise} \end{array}\right.$$

The right-hand side for the concentration equation $g^c_{j,k}$ is

$$g^c_{j,k} := (1-m)c^i_{j,k} - \bar{\rho}^i_{j,k} \tag{1.8}$$

The scheme (1.4) is positivity preserving. The proof is similar to the proof, for example, in [11]. For the readers convenience, we will give below a brief discussion of the positivity preserving property of the scheme.

Theorem 1.1 *Consider Patlak-Keller-Segel system (1.1) and the upwind scheme (1.4) with a positivity preserving piecewise linear reconstruction for* ρ. *Then, the computed cell densities* $\bar{\rho}^{i+1}_{j,k}$ *will be nonnegative provided that* $\bar{\rho}^i_{j,k}$ *are nonnegative and the following CFL condition is satisfied:*

$$\Delta t \le min\Big\{\frac{\Delta x}{4(\chi \cdot amax)}, \frac{\Delta y}{4(\chi \cdot bmax)}\Big\} \tag{1.9}$$

where

$$amax := \max_{j,k}\left|\frac{c^i_{j+1,k} - c^i_{j,k}}{\Delta x}\right|, \quad bmax := \max_{j,k}\left|\frac{c^i_{j,k+1} - c^i_{j,k}}{\Delta y}\right|$$

Proof: Similar to [11], we can use the conservation property of the reconstruction for ρ (1.7) and rewrite:

$$\bar{\rho}^i_{j,k} = \frac{1}{4}\Big(\widetilde{\rho}^i(x_{j+\frac{1}{2}} - 0, y_k) + \widetilde{\rho}^i(x_{j-\frac{1}{2}} + 0, y_k) + \widetilde{\rho}^i(x_j, y_{k+\frac{1}{2}} - 0) + \widetilde{\rho}^i(x_j, y_{k-\frac{1}{2}} + 0)\Big).$$

From this representation and from the definition of the upwind fluxes (1.6), it follows that the coefficients in front of $\rho^{E,W,N,S}_{j,k} := \{\widetilde{\rho}^i(x_{j+\frac{1}{2}}-0, y_k), \widetilde{\rho}^i(x_{j-\frac{1}{2}}+0, y_k), \widetilde{\rho}^i(x_j, y_{k+\frac{1}{2}}-0), \widetilde{\rho}^i(x_j, y_{k-\frac{1}{2}}+0)\}$ will be nonnegative if (1.9) is satisfied.

Now, we can rewrite the equation for $\bar{\rho}$ in the scheme (1.4) in the following form:

$$(I + \Delta t M)\rho^{\mathbf{i+1}}_{\mathbf{v}} = \vec{R}(\rho^{E,W,N,S}), \tag{1.10}$$

where M is a M-matrix ([26]), $\rho^{\mathbf{i+1}}_{\mathbf{v}}$ is a vector containing the cell averages $\bar{\rho}^{i+1}_{j,k}$ and $\vec{R}$ is a vector with nonnegative components under the CFL condition (1.9). From this, we can conclude that all the components of the solution $\rho^{\mathbf{i+1}}_{\mathbf{v}}$ to the linear system (1.10) are also nonnegative. ☐

Remark:

The upper bound on the time step in (1.9) is a minimum of two terms $\Delta x/4(\chi \cdot amax)$ and$\Delta y/4(\chi \cdot bmax)$ which are related to the chemotaxis term in the equation for the cell density (1.1). In numerical experiments in Section 2, the time step is adapted based on condition (1.9):

near blow up $amax$ and $bmax$ become large and the time step for the implict-explicit scheme considered here is comparable to the time step of the explicit scheme (see for example theoretical estimate for the time step of the method developed in [11]). However, when $amax$ and $bmax$ are relatively small, the size of the time step in the explicit scheme (see [11]) is controlled by the parabolic term in the equation for the density ρ, and the explicit time scheme becomes less efficient than the considered implicit-explicit method.

1.3 Difference Potentials - An Overview

We are concerned here with the Patlak-Keller-Segel system (1.1) in some domain Ω - an arbitrary bounded domain in $\mathbb{R}^2$ with the boundary $\partial\Omega$. We will employ the idea of the Difference Potentials Method (DPM) [40] as a part of our method and we will present below the overview about Difference

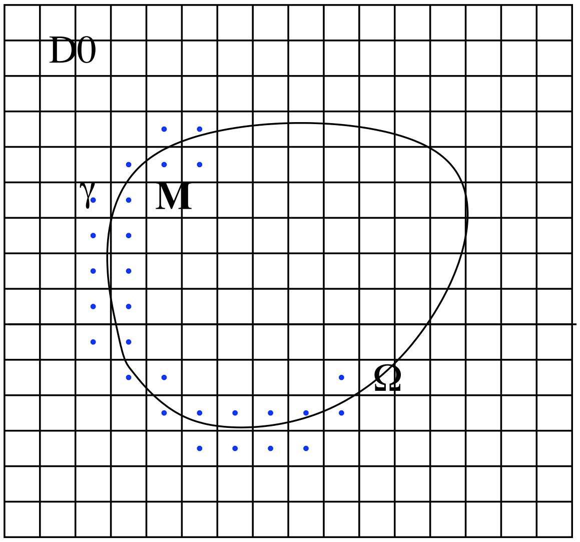

Figure 1: Example (a sketch) of the auxiliary domain D^0, original domain Ω; the example of some points (x_j, y_k)(-centers of the grid cells) in the set γ: the points which are outside Ω are from γ_{ex}, the points which are inside Ω are from $\gamma_{in} \in M$

Potential. For the readers convenience, we will also present the proofs of some facts in Appendix Sections 3. For the detailed discussion on DPM, see [40] (or for a brief introduction see, for example, [39]).

We introduce the auxiliary difference problem. Let us place the original domain Ω in the auxiliary domain $D^0 \subset \mathbb{R}^2$. The choice of the domain D^0 should be convenient for computations so we will choose it to be a square, and we will introduce a Cartesian mesh for D^0 consisting of the uniform cells $D^0_{j,k} := [x_{j-\frac{1}{2}}, x_{j+\frac{1}{2}}] \times [y_{k-\frac{1}{2}}, y_{k+\frac{1}{2}}]$ of the size $\Delta x \Delta y$ centered at the point $(x_j := j\Delta x, y_k := k\Delta y)$. Let us define a five-point stencil $N_{j,k}$ with its center placed at (x_j, y_k) to be the set of the following points: $N_{j,k} := \{(x_j, y_k), (x_{j\pm1}, y_k), (x_j, y_{k\pm1})\}$.

In addition, let us also introduce point sets $M := M^\rho = M^c := (x_j, y_k) \in \Omega$ - the sets of all the points (x_j, y_k) that belong to the interior of the original domain Ω. We now define $N := N^\rho = N^c = \{\bigcup_{j,k} N_{j,k} | (x_j, y_k) \in M\}$- the set of all points covered by five-point stencils when center point (x_j, y_k) of the stencil goes through all the points of the set M.

Let us remark, that points in the set N will be both inside and outside of the original domain Ω. Also, let us mention that index ρ and c were used to emphasize that in general we can have different grids for the numerical approximation of the density and concentration but in this work we consider the same grid.

Now, let us introduce the grid boundaries $\gamma_{ex} := \gamma^\rho_{ex} = \gamma^c_{ex} := N \backslash M$- exterior grid boundary layer for domain Ω, $\gamma_{in} := \gamma^\rho_{in} = \gamma^c_{in} := \{(x_j, y_k) | (x_j, y_k) \in M : N_{j,k} \not\subset M\}$ - interior grid boundary layer for domain Ω and define $\gamma := \gamma_{ex} \cup \gamma_{in}$ - a narrow set of nodes which surrounds the continuous boundary $\partial\Omega$, Figure 1.3.

Let us also construct the auxiliary set $M^1 := M^{1,\rho} = M^{1,c}$ by completing the set N to a rectangle and adding one extra layer of grid points to each side of the rectangle, hence $N \subset M^1$. Also, as before, define $N^1 := N^{1,\rho} = N^{1,c} = \{\cup_{j,k} N_{j,k} | (x_j, y_k) \in M^1\}$ and finally, let us introduce $\gamma^1 := \gamma^{1,\rho} = \gamma^{1,c} = N^1 \backslash M^1$.

Based on a scheme (1.4), we will formulate now a *General Auxiliary Problem:*

For the given grid functions g^1 and g^2, find the solution of the scheme (f^1, f^2) such that:

$$\begin{aligned} \Delta_{j,k} f^1 - m f^1_{j,k} &= g^1_{j,k}, \quad (x_j, y_k) \in M_1, && (1.11)\\ f^1_{j,k} &= 0, \quad (x_j, y_k) \in \gamma^1 && (1.12) \end{aligned}$$

$$\begin{aligned} \Delta_{j,k} f^2 - m f^2_{j,k} &= g^2_{j,k}, \quad (x_j, y_k) \in M_1, && (1.13)\\ f^2_{j,k} &= 0, \quad (x_j, y_k) \in \gamma^1 && (1.14) \end{aligned}$$

We note that the *General Auxiliary Problem* (1.11)-(1.14) is well defined for any right hand side $g^1_{j,k}, g^2_{j,k}$ - it has a unique solution (f^1, f^2) defined on the set N^1.
Also, it can be noted that the solution of (1.11)-(1.14) can be efficiently computed using the Fast Fourier Transform (FFT) with the appropriate choice of the auxiliary set M^1.
Next, we denote by

$$\mathbf{f} := (f^{\bar{\rho}}, f^c) \tag{1.15}$$

the solution (f^1, f^2) of the auxiliary problem (1.11)-(1.14) when the right hand-sides are defined as

$$g^1_{j,k} := \begin{cases} g^{\rho}_{j,k}, & (x_j, y_k) \in M, \\ 0, & (x_j, y_k) \in M^1 \backslash M \end{cases} \tag{1.16}$$

and

$$g^2_{j,k} := \begin{cases} g^{c}_{j,k}, & (x_j, y_k) \in M, \\ 0, & (x_j, y_k) \in M^1 \backslash M \end{cases} \tag{1.17}$$

where $g^{\rho}_{j,k}$ and $g^c_{j,k}$ are given in (1.5) and (1.8).

We now introduce a linear space V_γ of all grid functions denoted by $\mathbf{v}_\gamma := (\bar{\rho}^\gamma, c^\gamma)$ defined on γ, similar to [40, 39]. We will extend by zero the value of $\mathbf{v}_\gamma$ to other points of the grid D^0.

Let us recall that, *Difference Potential* [40, 39] with the given density $\mathbf{v}_\gamma$ is the grid function $\mathbf{u} = (u_{\bar{\rho}}, u_c) := \mathbf{P}\mathbf{v}_\gamma$ which coincides with the solution of (1.11)-(1.14) with the right hand-side defined as follows:

$$g^1_{j,k} := \begin{cases} 0, & (x_j, y_k) \in M, \\ \Delta_{j,k}\bar{\rho}^\gamma - m\bar{\rho}^\gamma_{j,k}, & (x_j, y_k) \in M^1 \backslash M \end{cases} \tag{1.18}$$

and

$$g^2_{j,k} := \begin{cases} 0, & (x_j, y_k) \in M, \\ \Delta_{j,k} c^\gamma - m c^\gamma_{j,k}, & (x_j, y_k) \in M^1 \backslash M \end{cases} \tag{1.19}$$

Here, $\mathbf{P}$ denotes the operator which constructs difference potential $\mathbf{u} = \mathbf{P}\mathbf{v}_\gamma$ from the given density $\mathbf{v}_\gamma \in V_\gamma$. The operator $\mathbf{P}$ is the linear operator of the density $\mathbf{v}_\gamma$. Hence, it can be easily constructed following, for example, this idea [40]:

$$\begin{aligned} u^p_\rho &:= \sum_{l \in \gamma^\rho} R^\rho_{lp} \bar{\rho}^\gamma_l, \quad p := (j,k) \in N^\rho, && (1.20)\\ u^p_c &:= \sum_{l \in \gamma^c} C^c_{lp} c^\gamma_l, \quad p \in N^c. && (1.21) \end{aligned}$$

Here, by $(u^p_\rho,\ u^p_c)$ we denote the value at point p of the Difference Potential with the density $\mathbf{v}_\gamma = (\bar{\rho}^\gamma, c^\gamma)$ and R^ρ_{lp}, C^c_{lp} are the coefficients. For example, the coefficients R^ρ_{lp} can be computed by solving an auxiliary problem (1.11) - (1.12) with (1.18) (or by constructing a Difference Potential) with the unit density $\bar{\rho}^\gamma_l$ at point $l = l^\star := (j^\star, k^\star) \in \gamma^\rho$:

$$\bar{\rho}^\gamma_l = \begin{cases} 1, & l = l^\star := (j^\star, k^\star) \in \gamma^\rho, \\ 0, & \forall l \neq l^\star \in \gamma^\rho \end{cases} \tag{1.22}$$

Therefore, R^{ρ}_{lp} is the value of the solution at point $p \in N^{\rho}$ to (1.11) - (1.12) with the right hand-side defined in (1.18) where density is given in (1.22) (or the value of the Difference Potential with density (1.22) at point $p \in N^{\rho}$). Coefficients C^{c}_{lp} can be computed in exactly the same way.
Next, let us recall [40, 39] and define another operator $\mathbf{P}_{\gamma} : V_{\gamma} \to V_{\gamma}$ which is defined as the trace (or restriction) of the Difference Potential $\mathbf{P}\mathbf{v}_{\gamma}$ on the grid boundary γ: $\mathbf{P}_{\gamma} := Tr_{\gamma}\mathbf{P}\mathbf{v}_{\gamma} = \mathbf{P}\mathbf{v}_{\gamma}|_{\gamma}$. Let us now state an important theorem for our algorithm. The proof of this theorem is the direct application to our model and scheme of the original proof given in [40], and for the reader's convenience we will present it in Appendix 3.1:

Theorem 1.2 *At each time level density* $\mathbf{v}_{\gamma} = (\bar{\rho}^{\gamma}, c^{\gamma}) \in V_{\gamma}$ *is the trace of some solution* $\mathbf{u}^{\bar{\rho}\mathbf{c}} := (\bar{\rho}, c)$ *to the upwind scheme (1.4):* $\mathbf{v}_{\gamma} = Tr_{\gamma}\mathbf{u}^{\bar{\rho}\mathbf{c}}$, *if and only if we have*

$$\mathbf{v}_{\gamma} = \mathbf{P}_{\gamma}\mathbf{v}_{\gamma} + \mathbf{f}_{\gamma}, \tag{1.23}$$

where $\mathbf{f}_{\gamma} = \mathbf{Tr}_{\gamma}\mathbf{f}$ *and* f *is defined in (1.15).*

Proof:
See Appendix 3.1. ☐

Hence, this theorem implies that the unique solution $\mathbf{u}^{\mathbf{pks}} := (\bar{\rho}, c)$ to problem (1.4), subject to the boundary conditions on $\partial\Omega$, is the unique solution of the following problem (1.24) (and vice versa: the unique solution of the problem (1.24) is the unique solution to the problem (1.4) subject to the corresponding boundary conditions):

1. At time level t^{i+1} find the solution $\mathbf{f} = (f^{\bar{\rho}}, f^{c})$ of the auxiliary problem (1.11)-(1.14), (1.16)-(1.17)
2. Solve system of boundary equations for $\mathbf{v}_{\gamma}$ with the imposed boundary conditions:

$$\mathbf{v}_{\gamma} = P_{\gamma}\mathbf{v}_{\gamma} + \mathbf{f}_{\gamma}, \quad l(\mathbf{P}\mathbf{v}_{\gamma} + \mathbf{f}) = \psi \tag{1.24}$$

3. Construct difference potential $P\mathbf{v}_{\gamma}$ with the obtained density $\mathbf{v}_{\gamma}$
4. At each time level t^{i+1}: $\mathbf{u}^{\mathbf{pks}} = P\mathbf{v}_{\gamma} + \mathbf{f}$,

where $l(\mathbf{P}\mathbf{v}_{\gamma} + \mathbf{f}) = \psi$ is the approximation at the points of set γ of the zero Neumann boundary conditions for $(\bar{\rho}, c)$. This approximation can be obtained, for example, using either an interpolation idea to approximate $\frac{\partial\bar{\rho}}{\partial n}$ and $\frac{\partial c}{\partial n}$ at some points in set γ, or by using a spectral approximation approach to approximate the boundary conditions (which we discuss in Section 1.4).
At this point let us briefly review some properties of the boundary equations (1.23) with the given $\mathbf{f}$. These equations can be rewritten as the system of the linear equations for the unknown densities $(\bar{\rho}^{\gamma}_{p}, c^{\gamma}_{p}), \quad p := (j, k) \in \gamma$. Using representation (1.20) and (1.21) of the difference potential $\mathbf{P}\mathbf{v}_{\gamma}$ we obtain the following system of linear equations:

$$\bar{\rho}^{\gamma}_{p} - \sum_{l \in \gamma^{\rho}} R^{\rho}_{lp}\bar{\rho}^{\gamma}_{l} = f^{\bar{\rho}}_{p}, \quad p \in \gamma^{\rho} \tag{1.25}$$

$$c^{\gamma}_{p} - \sum_{l \in \gamma^{c}} C^{c}_{lp}c^{\gamma}_{l} = f^{c}_{p}, \quad p \in \gamma^{c} \tag{1.26}$$

Lemma 1.3 *The rank* r *of the system (1.25) - (1.26) is equal to* $|\gamma^{\rho}_{in}| + |\gamma^{c}_{in}|$.

Proof:
We briefly review the proof in Appendix 3.2. It follows the lines of the original one in [40]. ☐

Theorem 1.4 *The subsystem of the system (1.25) - (1.26):*

$$\bar{\rho}_p^{\gamma} - \sum_{l\in\gamma^\rho} R_{lp}^{\rho}\bar{\rho}_l^{\gamma} = f_p^{\bar{\rho}}, \quad p \in \gamma_{in}^{\rho} \tag{1.27}$$

$$c_p^{\gamma} - \sum_{l\in\gamma^c} C_{lp}^{c} c_l^{\gamma} = f_p^{c}, \quad p \in \gamma_{in}^{c} \tag{1.28}$$

is equivalent to the original system (1.25) - (1.26) and it consists of linearly independent equations.

Proof:
The proof follows the lines of the one in [40], and for readers' convenience, we briefly recall it in Appendix 3.3. ☐

1.4 System of Boundary Equations

In this section we will assume that the solution is given at a fixed time level and we will suppress for the clarity of the presentation below the explicit dependence on time.
As we already showed in Section 1.3, the unique solution $\mathbf{u}^{\mathbf{pks}} := (\bar{\rho}, c)$ to the original Patlak-Keller-Segel problem (1.4), subject to zero Neumann boundary conditions on $\partial\Omega$, is the unique solution of problem (1.24) (and vice versa). Let us consider the system of boundary equations with the imposed boundary conditions at step 2 in the problem (1.24):

$$\begin{cases} \bar{\rho}_p^{\gamma} - \sum_{l\in\gamma^\rho} R_{lp}^{\rho}\bar{\rho}_l^{\gamma} = f_p^{\bar{\rho}}, \quad p \in \gamma_{in}^{\rho} \\ c_p^{\gamma} - \sum_{l\in\gamma^c} C_{lp}^{c} c_l^{\gamma} = f_p^{c}, \quad p \in \gamma_{in}^{c} \end{cases} \tag{1.29}$$

$$l((\bar{\rho}^{\gamma}, c^{\gamma})) = \psi \tag{1.30}$$

- where R_{lp}^{ρ} and C_{lp}^{c} are the given coefficients (see (1.20)-(1.22) in Section 1.3 for details)
- $l(\bar{\rho}^{\gamma}, c^{\gamma}) = \psi$ is the proper approximation (which is discussed below) of the zero Neumann boundary conditions for $(\bar{\rho}, c)$ at the points of set γ.
- $(f_p^{\bar{\rho}}, f_p^{c})$ is the restriction to the grid boundary γ_{in} of the solution to the auxiliary problem (1.11)-(1.14) with the right hand-sides defined in (1.16)-(1.17).
- the unknowns $(\bar{\rho}^{\gamma}, c^{\gamma})$ are the traces of the solutions $\mathbf{u}^{\mathbf{pks}} = (\bar{\rho}, c)$ on the corresponding grid boundaries.

In (1.29) we have system of $|\gamma_{in}^{\rho}| + |\gamma_{in}^{c}|$ equations for $|\gamma^{\rho}| + |\gamma^{c}|$ unknowns. The additional equations/conditions will be obtained from the approximation of the boundary conditions (1.30), $l((\bar{\rho}^{\gamma}, c^{\gamma})) = \psi$. Below we discuss two possible approaches for such approximations:

- *Simple Geometry - Rectangular Domain*
  We will illustrate our idea with the help of Figure 2. Assume for example, that point $(j^\star, k^\star) \in \gamma_{in}$ and the neighboring point $(j^\star + 1, k^\star) \in \gamma_{ex}$. Since in this paper we are concerned with zero Neumann boundary conditions $\frac{\partial\bar{\rho}}{\partial n} = 0$, $\frac{\partial c}{\partial n} = 0$, and in this case with simple geometry, we can assume with the second order of accuracy that

$$\bar{\rho}_{j^\star+1,k^\star}^{\gamma} = \bar{\rho}_{j^\star,k^\star}^{\gamma} \tag{1.31}$$

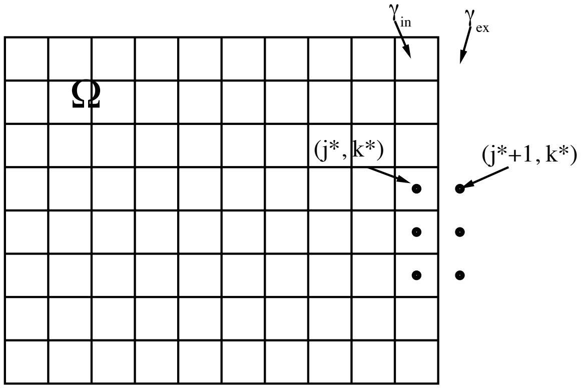

Figure 2: *Example (a sketch) of the simple geometry* Ω*; point* $(x^\star_j, y^\star_k)$ *is in the set* $\gamma_{in} \in M$*, the neighboring point* $(x_{j^\star+1}, y_{k^\star})$ *is from* γ_{ex}*.*

and similarly

$$c^\gamma_{j^\star+1,k^\star} = c^\gamma_{j^\star,k^\star} \tag{1.32}$$

Hence, due to these relations, we will have only $|\gamma^\rho_{in}| + |\gamma^c_{in}|$ unknowns in system (1.29) - the values of $\bar{\rho}^\gamma$ and c^γ at points in γ_{in}.

- *Complex Geometry - Curve Boundary*
  First, let us note that the finite difference approximation can be developed in this case as well for (1.30). However, we will consider a spectral approach instead for the approximation of the boundary conditions (see for example [39]). This approach is more computationally efficient and less technical.
  Assume that the continuous density ρ and its normal derivative $\frac{\partial\rho}{\partial n}$ on the boundary of the domain $\partial\Omega$ are functions of the parameter s - arc length

$$\rho|_{\partial\Omega} := \rho_\Gamma(s), \quad \left.\frac{\partial\rho}{\partial n}\right|_{\partial\Omega} := \rho^n_\Gamma(s) = 0 \tag{1.33}$$

Similarly for the continuous concentration c:

$$c|_{\partial\Omega} := c_\Gamma(s), \quad \left.\frac{\partial c}{\partial n}\right|_{\partial\Omega} := c^n_\Gamma(s) = 0 \tag{1.34}$$

Therefore we can express the point values of $\rho_p, \quad p = (j,k) \in \gamma^\rho$ and $c_p, \quad p \in \gamma^c$ using Taylor's expansion with respect to the shortest distance $d_{j,k}$ from the point $p \in \gamma$ to the boundary $\partial\Omega$, Figure 3 :

$$\rho(x_j, y_k) = \rho_\Gamma(s_{j,k}) + O(d^2_{j,k}) \text{ and } \rho_{j,k} \approx \rho_\Gamma(s_{j,k}) \tag{1.35}$$

$$c(x_j, y_k) = c_\Gamma(s_{j,k}) + O(d^2_{j,k}) \text{ and } c_{j,k} \approx c_\Gamma(s_{j,k}), \tag{1.36}$$

here and below by $s_q \in \Gamma$, we denote the point of intersection of normal with the boundary Γ (the normal is constructed from the grid point q to the boundary Γ in the direction of the shortest distance). Note that from the definition of the set γ, we have that $O(d_{j,k}) = O(h)$.

Also, let us notice that the cell average value $\bar{\rho}_{j,k}$ is equal to the value at the center of the cell

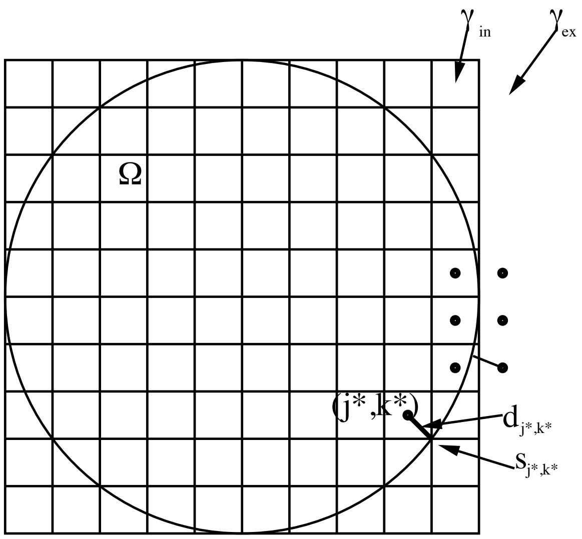

Figure 3: *Example (a sketch) of the geometry with the curve boundary* Ω*; point* $(x^\star_j, y^\star_k)$ *is in the set* $\gamma_{in} \in M$*,* $d_{j*,k*}$ *is the distance from this point to the boundary of the domain* Ω*, and* $s_{j^\star,k^\star}$ *is the corresponding arc length.*

$\rho(x_j, y_k)$ with the second order accuracy,

$$\bar{\rho}_{j,k} = \rho(x_j, y_k) + O(h^2) \tag{1.37}$$

Therefore, we have

$$\bar{\rho}_{j,k} \approx \rho_\Gamma(s_{j,k}), \tag{1.38}$$
$$c_{j,k} \approx c_\Gamma(s_{j,k}) \tag{1.39}$$

Alternatively, one can express cell averages using Simpson's rule:

$$\bar{\rho}_{j,k} = (16\rho(x_j, y_k) + 4(\rho(x_{j-\frac{1}{2}}, y_k) + \rho(x_{j+\frac{1}{2}}, y_k) + \rho(x_j, y_{k-\frac{1}{2}}) + \rho(x_j, y_{k+\frac{1}{2}}) + \tag{1.40}$$
$$\rho(x_{j-\frac{1}{2}}, y_{k-\frac{1}{2}}) + \rho(x_{j+\frac{1}{2}}, y_{k-\frac{1}{2}}) + \rho(x_{j-\frac{1}{2}}, y_{k+\frac{1}{2}}) + \rho(x_{j+\frac{1}{2}}, y_{k+\frac{1}{2}}))/36 + O(h^4) \tag{1.41}$$

Therefore, in this case we can obtain with the second order of accuracy (using Taylor's expansion, similar to formulas for $\rho(x_j, y_k)$ and $c(x_j, y_k)$ in (1.35) - (1.36)), that

$$\bar{\rho}_{j,k} \approx (16\rho_\Gamma(s_{j,k}) + 4(\rho_\Gamma(s_{j-\frac{1}{2},k}) + \rho_\Gamma(s_{j+\frac{1}{2},k}) + \rho_\Gamma(s_{j,k-\frac{1}{2}}) + \rho_\Gamma(s_{j,k+\frac{1}{2}})) + \tag{1.42}$$
$$\rho_\Gamma(s_{j-\frac{1}{2},k-\frac{1}{2}}) + \rho_\Gamma(s_{j+\frac{1}{2},k-\frac{1}{2}}) + \rho_\Gamma(s_{j-\frac{1}{2},k+\frac{1}{2}}) + \rho_\Gamma(s_{j+\frac{1}{2},k+\frac{1}{2}}))/36, \tag{1.43}$$

$$c_{j,k} \approx c_\Gamma(s_{j,k}), \tag{1.44}$$

Now, for the space defined on Γ of sufficiently smooth periodic functions of the arc length s, we introduce the set of the basis functions $\phi_n(s) := \phi^\rho_n = \phi^c_n$ defined on the boundary of the domain $\partial\Omega$. For example, one can consider

$$\phi_1(s) = 1, \quad \phi_2(s) = \cos\left(\frac{2\pi}{|\Gamma|}s\right), \quad \phi_3 = \sin\left(\frac{2\pi}{|\Gamma|}s\right), ...$$
$$\phi_{2N}(s) = \cos\left(\frac{2\pi}{|\Gamma|}Ns\right), \quad \phi_{2N+1} = \sin\left(\frac{2\pi}{|\Gamma|}Ns\right) \tag{1.45}$$

as the basis functions on $\partial\Omega$, and this is the set of the basis functions which we will use in our numerical experiments. We would like to note here that the set of basis functions can be different for the density ρ and concentration c approximations, but in our experiments we considered the same set of basis functions (1.45). Therefore, we can assume that

$$\rho_\Gamma(s) \approx \sum_{n=1}^{L} \widetilde{\rho}_n \phi_n(s), \tag{1.46}$$

$$c_\Gamma(s) \approx \sum_{n=1}^{L} \widetilde{c}_n \phi_n(s), \tag{1.47}$$

where L is the total number of the basis functions (it can also be chosen differently for the density and concentration approximations). Let us now consider, for example, approximation (1.38) -(1.39). Hence, from (1.46) - (1.47) we have that

$$\bar{\rho}^\gamma_{j,k} \approx \sum_{n=1}^{L} \widetilde{\rho}_n \phi_n(s_{j,k}) \tag{1.48}$$

$$c^\gamma_{j,k} \approx \sum_{n=1}^{L} \widetilde{c}_n \phi_n(s_{j,k}), \tag{1.49}$$

Therefore, if we know the expansion coefficients $\widetilde{\rho}_n$ and $\widetilde{c}_n$ in (1.48) - (1.49), we can obtain the approximation for $\bar{\rho}^\gamma$ and c^γ.

In order to find the coefficients $\widetilde{\rho}_n$ and $\widetilde{c}_n$, we consider the system of boundary conditions (1.29)-(1.30). Using (1.48) - (1.49) it can be rewritten as the system of linear equations for the unknown coefficients $\widetilde{\rho}_n$ and $\widetilde{c}_n$, $n = 1, .., L$.

First, we introduce the notation

$$u^p_{\phi^\rho_n} := \sum_{l\in\gamma^\rho} R^\rho_{lp} \phi_n(s_{j_l,k_l}), \tag{1.50}$$

$$u^p_{\phi^c_n} := \sum_{l\in\gamma^\rho} C^c_{lp} \phi_n(s_{j_l,k_l}), \tag{1.51}$$

here $u^p_{\phi^\rho_n}$ and $u^p_{\phi^c_n}$ are the values at the point p of the Difference Potentials with the density $\{\phi_n(s_{j_l,k_l}), \forall l \in \gamma\}$, where n is fixed. The values of $u^p_{\phi^\rho_n}$ and $u^p_{\phi^c_n}$ are computed using the definition of the Difference Potential (see Section 1.3). Therefore, they will be the known coefficients in the linear system presented below.

Hence, using (1.48) - (1.49) in (1.29) - (1.30), we obtain:

$$\sum_{n=1}^{L} (\phi^\rho_n(s_{j_p,k_p}) - u^p_{\phi^\rho_n})\widetilde{\rho}_n = f^{\bar{\rho}}_{j_p,k_p}, \quad p := (j_p, k_p) \in \gamma^\rho_{in}, \tag{1.52}$$

$$\sum_{n=1}^{L} (\phi^c_n(s_{j_p,k_p}) - u^p_{\phi^c_n})\widetilde{c}_n = f^c_{j_p,k_p}, \quad p \in \gamma^c_{in} \tag{1.53}$$

The above systems (1.52) - (1.53) are overdetermined since in general we need to have $L < |\gamma|$ for the accurate reconstruction of the $\bar{\rho}^\gamma$ and c^γ.

Let us denote the matrix (since we consider the same sets of basis functions for both ρ and c) of this systems by $A := A^{\rho} = A^{c} = \{a_{i,j}\} := (\phi_n(s_{j_p,k_p}) - u^{p}_{\phi_n}), \quad i = 1,..|\gamma|, j = 1,..L$, and right hand-sides by $y^{\bar{\rho}} := f^{\bar{\rho}}_{j_p,k_p}$ and $y^{c} := f^{c}_{j_p,k_p}$. Denote, $\widetilde{\rho} := \{\widetilde{\rho}_n\}$ and $\widetilde{\mathbf{c}} := \{\widetilde{c}_n\}, n = 1,..,L$ are the vectors with the components $\widetilde{\rho}_n$ and $\widetilde{c}_n$, $n = 1,..,L$:

$$A\widetilde{\rho} = y^{\bar{\rho}}, \tag{1.54}$$

$$A\widetilde{\mathbf{c}} = y^{c} \tag{1.55}$$

We solve these overdetermined systems (1.54) - (1.55) for $\widetilde{\rho}_n$ and $\widetilde{c}_n$, $n = 1,..,L$ using the standard least square method.

Remarks.

As usual, the spectral approach works very well when the solution is smooth, and it results in oscillations/ Gibbs phenomena when the solution loses its regularity. As expected, in our numerical experiments we observed that at a time very close to blow up time, we had to keep increasing the number of harmonics in order to obtain the solution without oscillations. However, on a given mesh the number of harmonics is limited by the condition $L < |\gamma|$. Hence, we have to introduce a modification in order to keep the solution without oscillations, even at post blow up times:

- One way is to refine the mesh: by doing so we can capture the solution accurately even at the later time.

- The other more efficient approach, which is the topic of our future investigations, is to design an adaptive procedure (for example some type of mesh redistribution near blowup). Here, we believe that we would be able to take advantage of our scheme: we obtain our solution in several steps (see Section 1.1) - as the sum of the solution to the auxiliary problem, as well as the Difference Potentials (see (1.3) in Section 1.1).

2 Numerical Examples

In this section we demonstrate the performance of our Upwind - Difference Potentials scheme on test problems. In the numerical experiments we used the upwind scheme (1.4) with the minmod limiter with $\theta = 2$

2.1 Validation of the Upwind-Difference Potentials Method on Patlak-Keller-Segel Chemotaxis Model with Radially Symmetric Initial Data in a Circle

As a first example, we consider the Patlak-Keller-Segel chemotaxis problem (1.1) -(1.2) in a circular domain $x^2 + y^2 = 0.25$ with the radially symmetric initial data:

$$\rho(x,y,0) = \rho_0 e^{-100(x^2+y^2)}, \quad c(x,y,0) = 0.5\rho_0 e^{-50(x^2+y^2)}, \tag{2.1}$$

where ρ_0 is the constant which will be specified later.

It has been proven (see, for example overview [24, 25]) that the solution to Patlak-Keller-Segel chemotaxis model with 'parabolic-parabolic' coupling in $\Omega \in \mathbb{R}^2$:

1. exists globally in time if the initial mass is $\int_{\Omega} \rho(x,y,0)dxdy < 4\pi$
2. is expected to blow up if the initial mass is $8\pi < \int_{\Omega} \rho(x,y,0)dxdy$

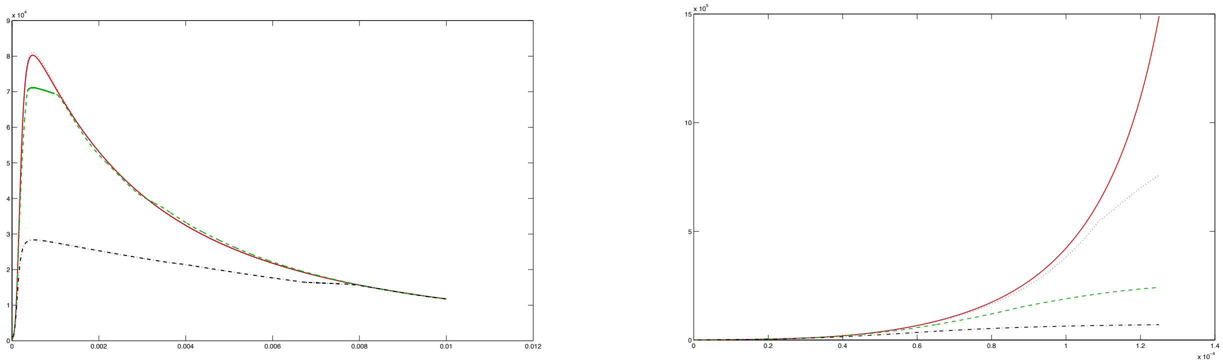

Figure 4: *Plots of* $\rho_{\max}(t)$ *- the evolution of the maximum value of the density* ρ *with time: left plot is for the case 1 with* $\rho_0 = 400$ *and the right plot is for the case 2 with* $\rho_0 = 850$*. Red solid line is* $\rho_{\max}(t)$ *computed on mesh* 507×507*; dotted blue is for* 251×251*; green dashed is for* 123×123*, and dark blue dash dotted is for* 59×59

We validate our scheme below by checking numerically properties (1) and (2).

For case (1) we set $\rho_0 = 400$ (plot of the initial data, Fig. 6) and we illustrate numerically (left plot on Fig. 4) that solution exists globally in time and we observe numerical convergence (Table 1, the proposed scheme is second order accurate but since we measure error at a particular point it can be greater than second order). For the case (2) we consider $\rho_0 = 850$ (plot of the initial data, Fig. 7) and we show that the proposed scheme will break the symmetry and the solution will approach the blow up (right plot on Fig. 4) and will blow up at the center of the circular domain as expected by the theory (Fig. 5 - density ρ at time around the blow-up time). We also observe here the deterioration of the numerical convergence of the scheme when solution gets closer and closer to the blowup (Table 2).

In Fig. 4 we plot the evolution of the maximum value of the density ρ with time

$$\rho_{\max}(t) := \max_{(x,y)} \rho(x,y,t)$$

on four different meshes - mesh 59×59, 123×123, 251×251 and 507×507.
In Tables 1 and 2 we compute relative error as

$$Error_{rel} := \frac{||\rho_{\max}(t) - \rho^\star_{\max}(t)||_2}{||\rho^\star_{\max}(t)||_2} = \frac{(\sum_{i=1}^N \Delta t(\rho_{\max}(t_i) - \rho^\star_{\max}(t_i))^2)^{1/2}}{(\sum_{i=1}^N \Delta t(\rho^\star_{\max}(t_i))^2)^{1/2}},$$

here by $||\cdot||_2$ we denote the L_2 norm with respect to time variable t and by $\rho^\star_{\max}(t)$ - the maximum value of the density at time t of the reference solution computed on mesh 507×507. The time step Δt here was set to $\Delta t = 2.0 \cdot 10^{-7}$ and it was selected based on the value of the smallest time step used to simulate the reference solution on mesh 507×507. Since the exact solution is not known we test the error against the reference solution computed on the fine mesh.

2.2 Example: Simple Geometry, Blowup at the Corner of a Square Domain

We consider the Patlak-Keller-Segel chemotaxis problem (1.1) -(1.2) in a square domain $[-0.5, 0.5] \times [-0.5, 0.5]$ with the initial conditions:

$$\rho(x,y,0) = 1000e^{-100((x-0.15)^2+(y-0.15)^2)}, \quad c(x,y,0) = 0 \tag{2.2}$$

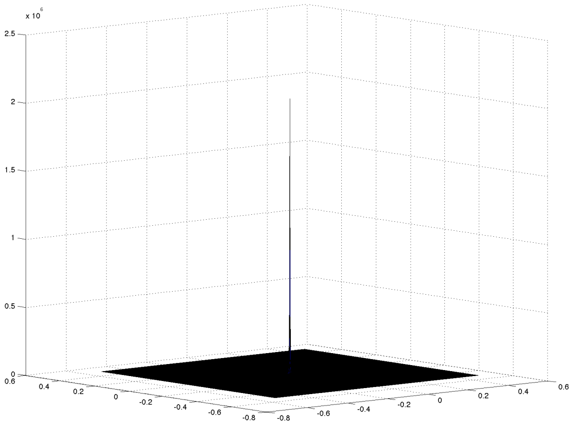

Figure 5: *Plot of the density* ρ *for the case 2 with* $\rho_0 = 850$ *at time around the blow up time* $t \approx 0.00013$*. The solution is computed on mesh* 507×507

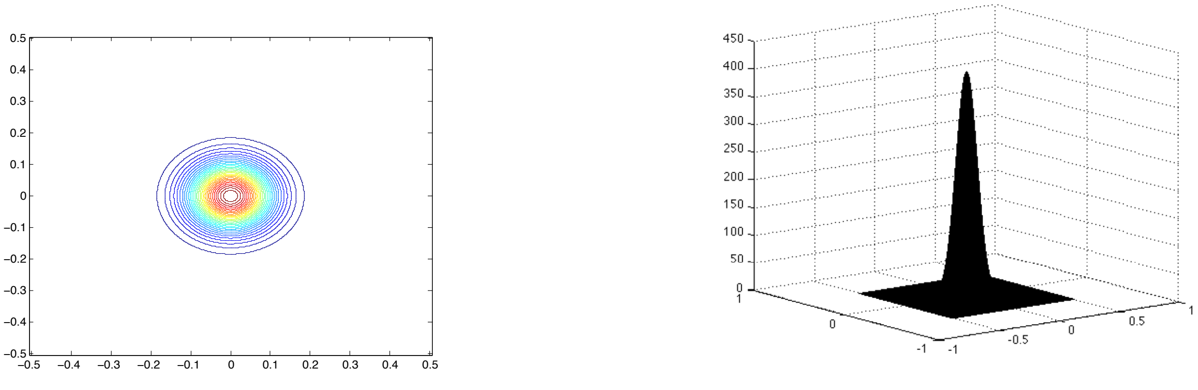

Figure 6: *Plot of the initial data* $\rho(x, y, 0)$ *with initial mass below* 4π

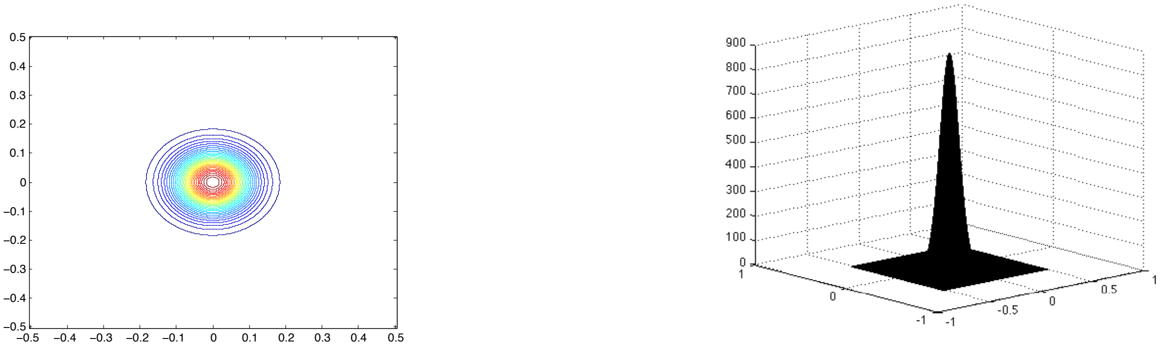

Figure 7: *Plot of the initial data $\rho(x, y, 0)$ with initial mass above 8π*

	Relative $L_2(t)$ error of $\rho_{\max}(t)$	Rate
1/59	0.52037	
1/123	0.05446	3.26
1/251	0.00573	3.25

Table 1: *Errors as functions of the mesh size h; reference solution is computed on mesh* 507×507. *Initial mass is below the critical mass*

	Relative $L_2(t)$ error of $\rho_{\max}(t)$	Rate
1/59	0.91368	
1/123	0.73783	0.31
1/251	0.33453	1.14

Table 2: *Errors as functions of the mesh size h; reference solution is computed on mesh* 507×507. *Initial mass is above the critical mass*

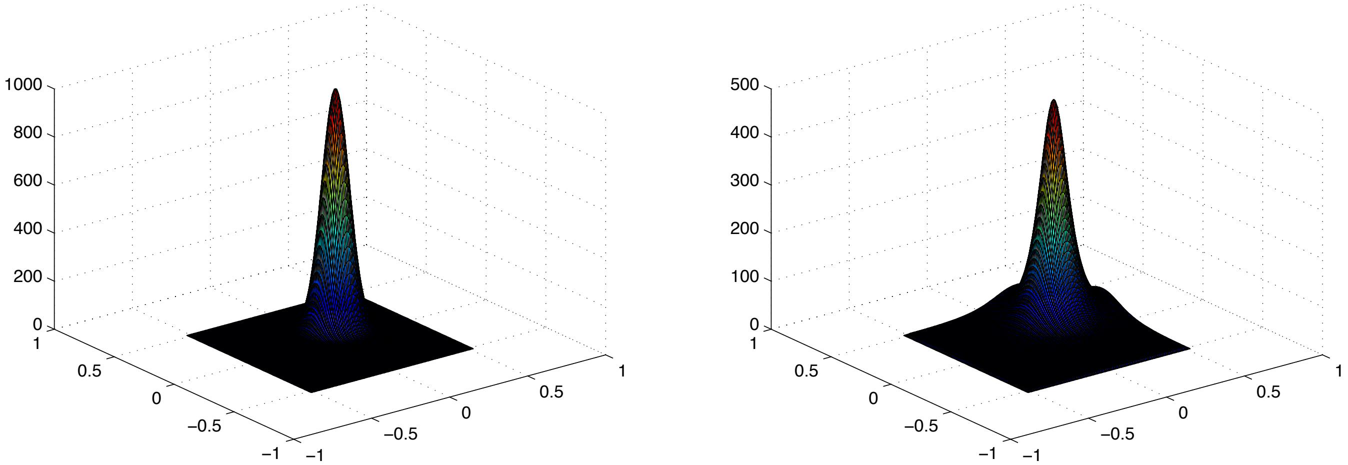

Figure 8: *Density ρ obtained by the proposed upwind-difference potentials method for the Patlak-Keller-Segel system at a initial time (left) and time before the blow up $t = 7.9 \cdot 10^{-2}$ (right). Mesh is 123×123 rectangles.*

It has been proven in [23] that in this case, the solution is expected to blow up at the boundary of the domain. We simulate this initial value problem on two different meshes: mesh with 123×123 rectangles and mesh with 251×251 rectangles. We observe from Figures 8 -11 that the proposed upwind-difference potentials scheme captures the dynamics and sharp gradients of the solution accurately. The solution moves to the boundary for the initial data (2.2) and blows up at the corner of the domain at a much later time than for the example in Section 2.1, since $c(x, y, 0) = 0$ here. We also notice that on the finer mesh Figures 10 -11 our scheme gives better resolution as expected.

2.3 Example: Geometry with Curved Boundary, Blowup at the Boundary of a Circle

We consider here the Patlak-Keller-Segel chemotaxis problem (1.1) -(1.2) in a circular domain $x^2 + y^2 = 0.25$ with the initial conditions:

$$\rho(x, y, 0) = 1000e^{-100((x-0.15)^2+(y-0.15)^2)}, \quad c(x, y, 0) = 0 \tag{2.3}$$

The solution is expected to blow up at the boundary of the domain. We consider for this example a fixed mesh with 251×251 rectangles. We use spectral approximation for the boundary conditions with total number of harmonics $L = 339$ (Figures 12 -15) and $L = 659$ (Figures 16 -19). We consider here (1.38)-(1.39) for the cell average approximation. We did not notice much difference in the results when we considered the approximation (1.42)-(1.43). We observe from Figures 12 -19 that the upwind-difference potentials scheme gives good approximation of the dynamics and sharp gradients. The solution moves in the radial direction to the boundary and blows up at the boundary in a finite time. We also notice that the approximation with greater number of harmonics $L = 659$ (Figures 16 -19) produces better resolution of the pre-blow up and blow up solution. Also, we observe from this experiment that the approximation with more harmonics affects the approximation of the blow up time.

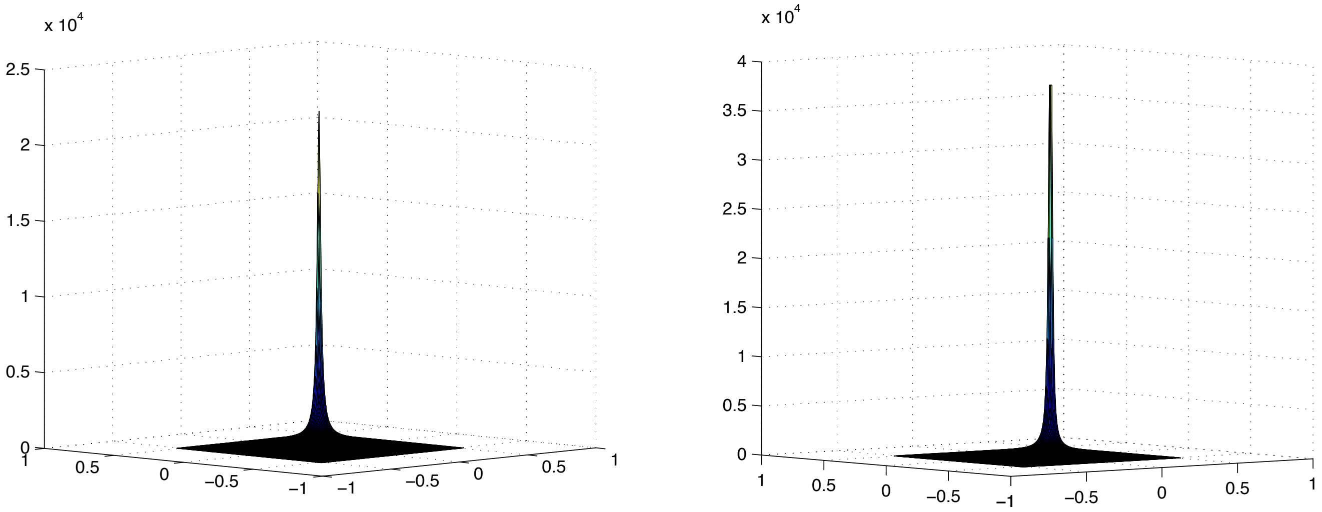

Figure 9: *Density ρ obtained by the proposed upwind-difference potentials method for the Patlak-Keller-Segel system at time near the blow up $t = 1.61 \cdot 10^{-1}$. Mesh is 123×123 rectangles.*

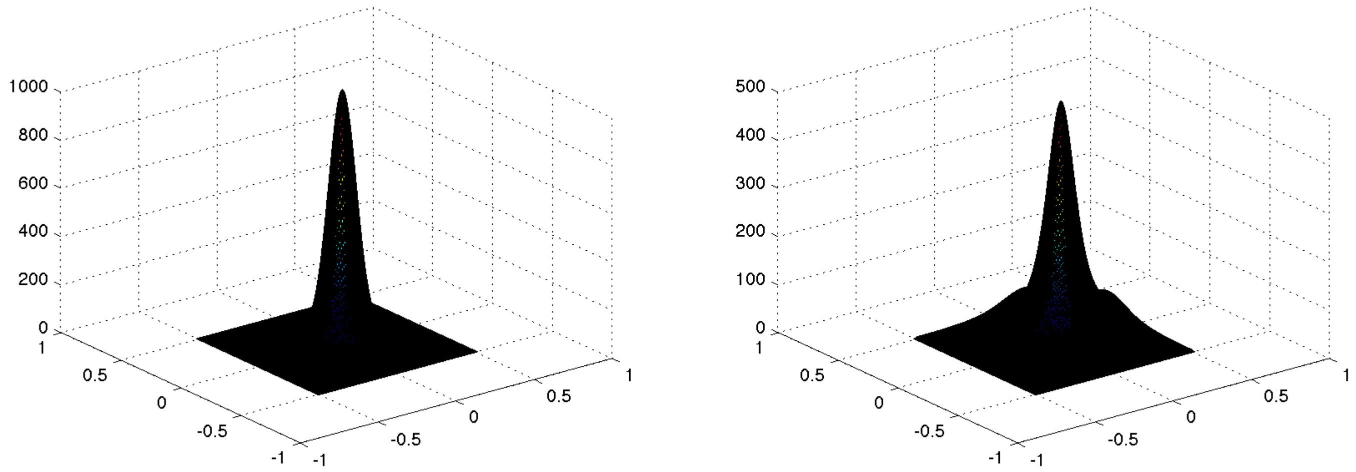

Figure 10: *Density ρ obtained by the proposed upwind-difference potentials method for the Patlak-Keller-Segel system at a initial time (left) and time before the blow up $t = 7.9 \cdot 10^{-2}$ (right). Mesh is 251×251 rectangles.*

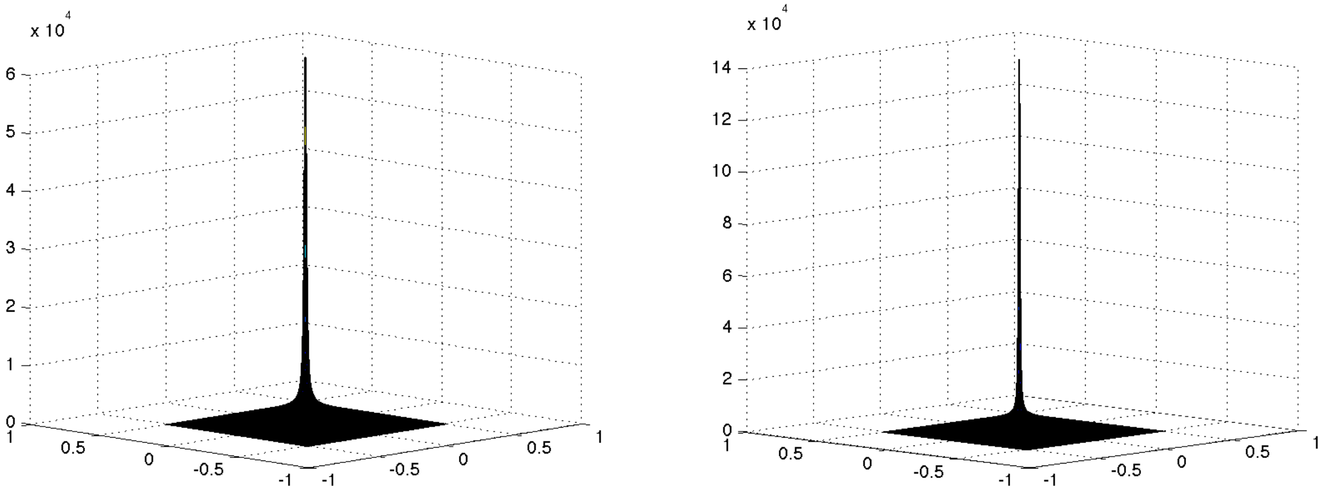

Figure 11: *Density ρ obtained by the proposed upwind-difference potentials method for the Patlak-Keller-Segel system at time near the blow up $t = 1.61 \cdot 10^{-1}$. Mesh is 251×251 rectangles.*

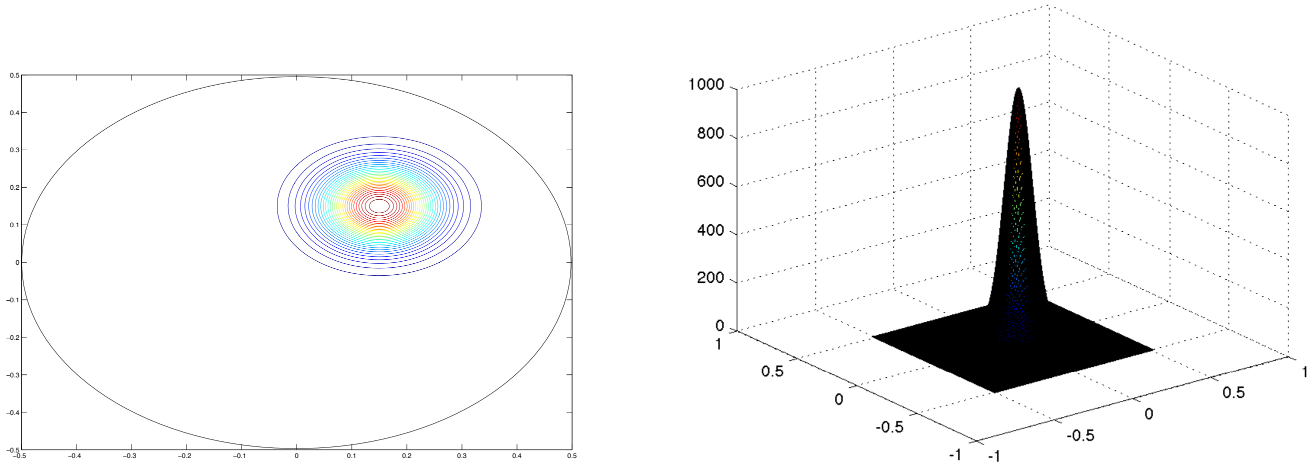

Figure 12: *Density ρ obtained by the proposed upwind-difference potentials method for the Patlak-Keller-Segel system at a initial time, $2D$ view - contour view (left) and $3D$ view (right). The total number of harmonics is $L = 339$.*

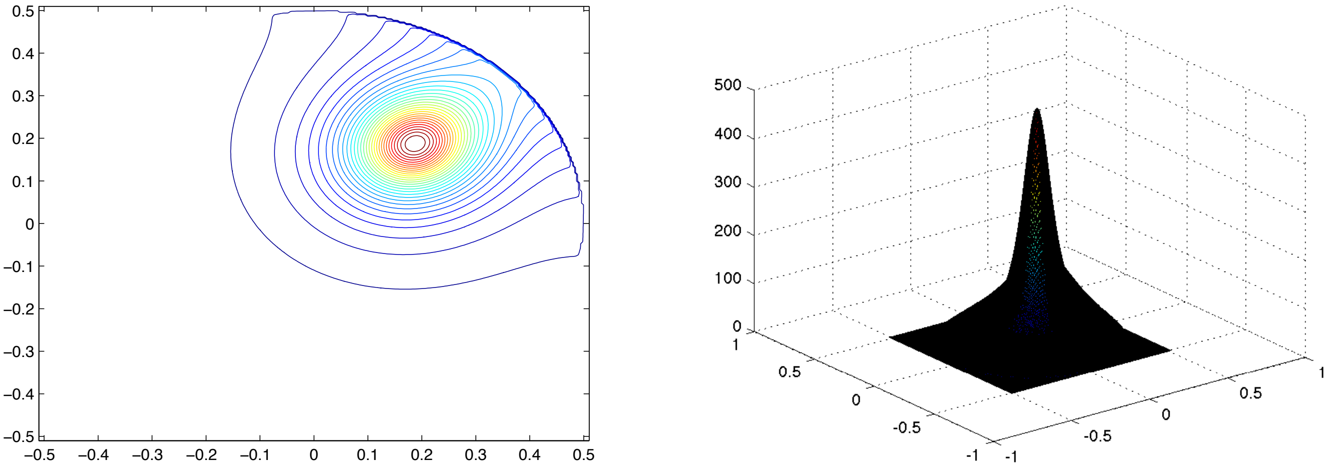

Figure 13: *Density ρ obtained by the proposed upwind-difference potentials method for the Patlak-Keller-Segel system at time before the blow up $t = 5.06 \cdot 10^{-2}$, 2D view - contour view (left) and 3D view (right). The total number of harmonics is $L = 339$.*

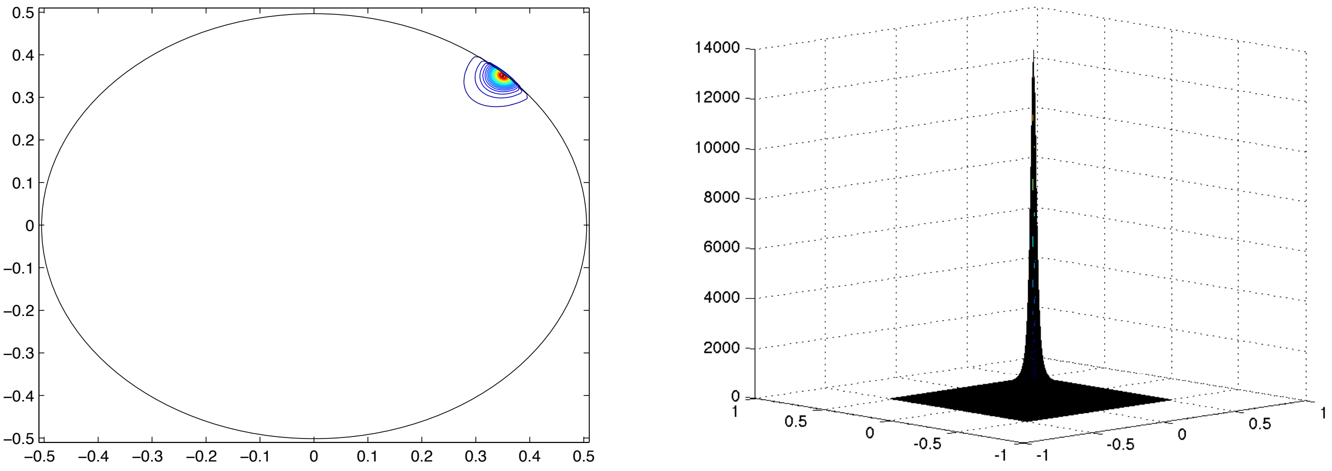

Figure 14: *Density ρ obtained by the proposed upwind-difference potentials method for the Patlak-Keller-Segel system at time near the blow up $t = 8.79 \cdot 10^{-2}$, 2D view -contour view (left) and 3D view (right). The total number of harmonics is $L = 339$.*

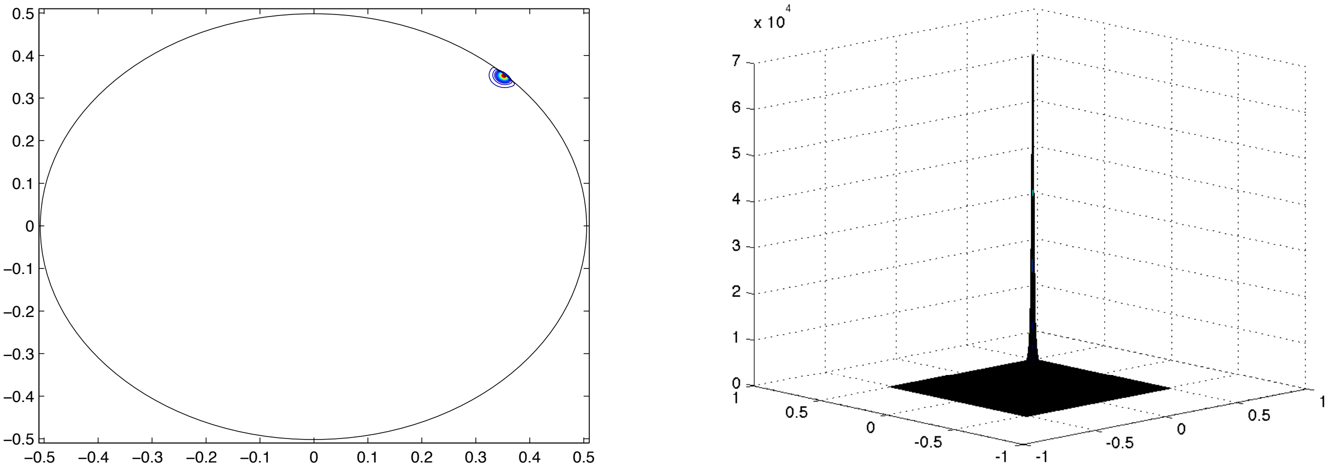

Figure 15: *Density ρ obtained by the proposed upwind-difference potentials method for the Patlak-Keller-Segel system at time close to blow up $t = 8.87 \cdot 10^{-2}$, 2D view - contour view (left) and 3D view (right). The total number of harmonics is $L = 339$. It is about 0.001 difference in time with the previous solution shown in Figure 14 but the maximum value of the solution changed by $O(10^4)$.*

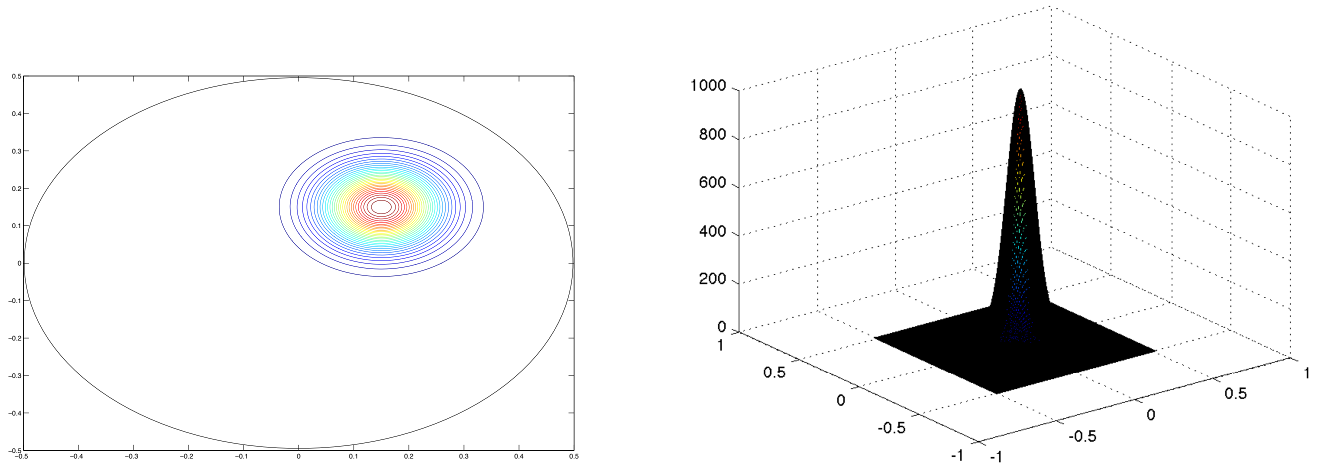

Figure 16: *Density ρ obtained by the proposed upwind-difference potentials method for the Patlak-Keller-Segel system at an initial time, 2D view - contour view (left) and 3D view (right). The total number of harmonics is $L = 659$.*

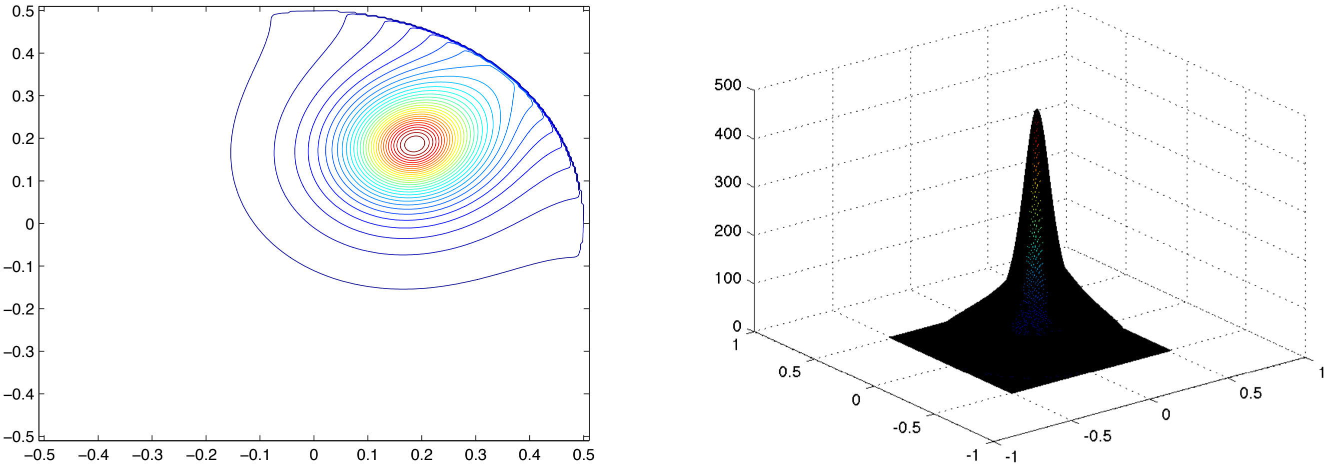

Figure 17: *Density ρ obtained by the proposed upwind-difference potentials method for the Patlak-Keller-Segel system at time before the blow up $t = 5.06 \cdot 10^{-2}$, $2D$ view - contour view (left) and $3D$ view (right). The total number of harmonics is $L = 659$*

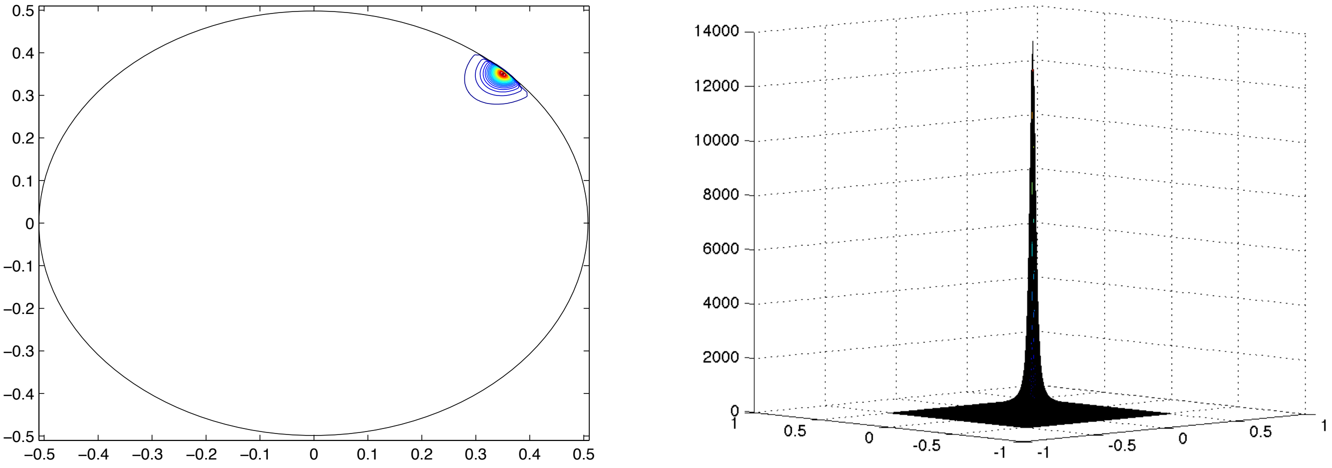

Figure 18: *Density ρ obtained by the proposed upwind-difference potentials method for the Patlak-Keller-Segel system at time near the blow up $t = 8.88 \cdot 10^{-2}$, $2D$ view -contour view (left) and $3D$ view (right). The total number of harmonics is $L = 659$.*

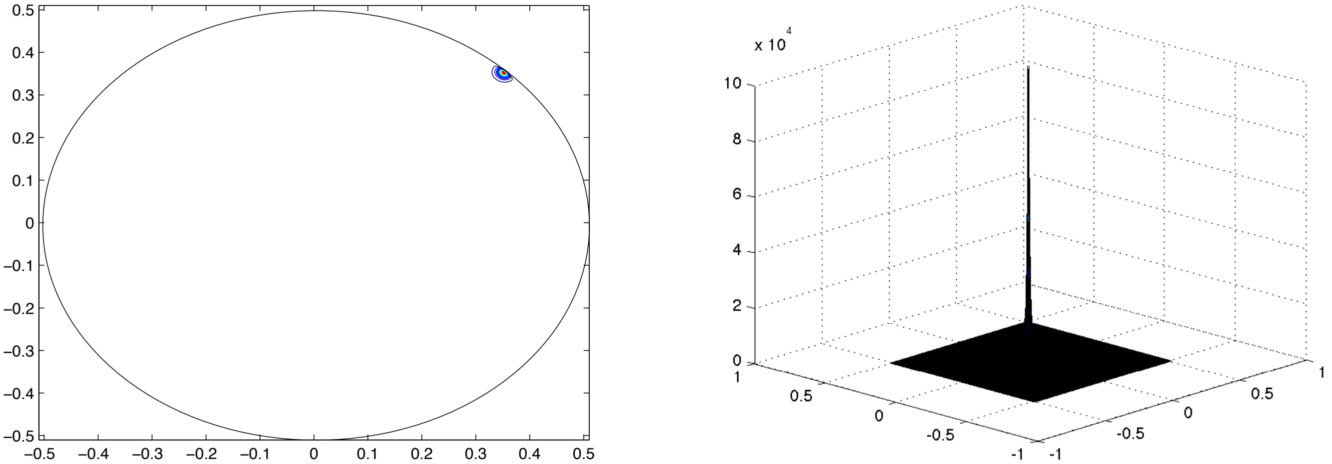

Figure 19: *Density ρ obtained by the proposed upwind-difference potentials method for the Patlak-Keller-Segel system at time close to blow up $t = 8.98 \cdot 10^{-2}$, 2D view - contour view (left) and 3D view (right). The total number of harmonics is $L = 659$. There is only a 0.001 difference in time with the previous solution shown in Figure 18, but the maximum value of the solution changed by $O(10^4)$.*

3 Appendix: Proof of Some Properties of the Difference Potentials

In this section, we briefly review for the reader's convenience the proofs of some properties of the Upwind-Difference Potentials method. The reader can consult book [40] for more detailed discussions on Difference Potentials Method and its applications.

3.1 Proof of the Main Theorem 1.2 in Section 1.3

First, assume that for some density $\mathbf{v}_\gamma = (\bar{\rho}^\gamma, c^\gamma) \in V_\gamma$ the relation (1.23) holds true. Now, let us construct function $\mathbf{u}^{\rho\mathbf{c}} := \mathbf{P}\mathbf{v}_\gamma + \mathbf{f}$. Hence, from the definitions in Section 1.3 of the Difference Potential $\mathbf{P}\mathbf{v}_\gamma$ and function $\mathbf{f}$, it follows that $\mathbf{u}^{\bar{\rho}\mathbf{c}}$ is the solution of the auxiliary problem (1.11)-(1.14) with the right hand-sides g^1 and g^2 given below:

$$g^1_{j,k} := \begin{cases} g^\rho_{j,k}, & (x_j, y_k) \in M, \\ \Delta_{j,k}\bar{\rho}^\gamma - m\bar{\rho}^\gamma_{j,k}, & (x_j, y_k) \in M^1 \backslash M \end{cases} \tag{3.1}$$

and

$$g^2_{j,k} := \begin{cases} g^c_{j,k}, & (x_j, y_k) \in M, \\ \Delta_{j,k}c^\gamma - mc^\gamma_{j,k}, & (x_j, y_k) \in M^1 \backslash M \end{cases} \tag{3.2}$$

here $g^\rho_{j,k}$ and $g^c_{j,k}$ are defined in (1.5) and (1.8) respectively. From this, it implies that $\mathbf{u}^{\rho\mathbf{c}} = \mathbf{P}\mathbf{v}_\gamma + \mathbf{f}$ is some solution to the upwind scheme (1.4). Therefore, density $\mathbf{v}_\gamma$ in (1.23) is the trace of some solution $\mathbf{u}^{\bar{\rho}\mathbf{c}}$ of (1.4) since $\mathbf{u}^{\bar{\rho}\mathbf{c}}|_\gamma = Tr_\gamma(\mathbf{P}\mathbf{v}_\gamma + \mathbf{f}) = \mathbf{P}_\gamma\mathbf{v}_\gamma + \mathbf{f}_\gamma = \mathbf{v}_\gamma$.

Now, let us assume that $\mathbf{v}_\gamma = Tr_\gamma \mathbf{u}^{\bar{\rho}\mathbf{c}} \in V_\gamma$ is the trace of some solution $\mathbf{u}^{\bar{\rho}\mathbf{c}} = (\bar{\rho}, c)$ of the upwind scheme (1.4). Again, construct the function $\mathbf{P}\mathbf{v}_\gamma + \mathbf{f}$ which will be the unique solution to the auxiliary problem (1.11)-(1.14) with the right-hand side (3.1) - (3.2). Since $\mathbf{v}_\gamma$ is the trace of $\mathbf{u}^{\bar{\rho}\mathbf{c}}$, and $\mathbf{u}^{\bar{\rho}\mathbf{c}}$ is the solution to the upwind scheme (1.4), we can express $g^1_{j,k}$ and $g^2_{j,k}$ in (3.1) - (3.2) for any $(x_j, y_k) \in M^1$ as:

$$g^1_{j,k} = \Delta_{j,k}\bar{\rho} - m\bar{\rho}_{j,k}, \tag{3.3}$$

$$g^2_{j,k} = \Delta_{j,k}c - mc_{j,k}, \tag{3.4}$$

where $\bar{\rho}$ and c denote the solution to the upwind scheme (1.4) at each time level. Hence, due to a uniqueness argument, $\mathbf{P}\mathbf{v}_\gamma + \mathbf{f}$ coincides with the solution $\mathbf{u}^{\bar{\rho}\mathbf{c}}$ of the upwind scheme (1.4): $\mathbf{u}^{\bar{\rho}\mathbf{c}} = \mathbf{P}\mathbf{v}_\gamma + \mathbf{f}$. From this we conclude that the trace $\mathbf{v}_\gamma$ of the solution $\mathbf{u}^{\bar{\rho}\mathbf{c}}$ to the upwind scheme (1.4) can be reconstructed from the formula: $\mathbf{v}_\gamma = Tr_\gamma \mathbf{u}^{\bar{\rho}\mathbf{c}} = \mathbf{P}_\gamma \mathbf{v}_\gamma + \mathbf{f}_\gamma$. ☐

3.2 Proof of the Lemma 1.3 in Section 1.3

This can be shown by recalling that the upwind scheme (1.4) has a unique solution if $\bar{\rho}_p$ and c_p are defined for all points $p \in \gamma^\rho_{ex}$ and $p \in \gamma^c_{ex}$ respectively. It implies that the dimension of the solution space to (1.4) is $|\gamma^\rho_{ex}| + |\gamma^c_{ex}|$. Since the unique solution to problem (1.24) is the unique solution to the scheme (1.4) with the appropriate boundary conditions and since the functions are constructed uniquely at steps 1, 2 and 4 of the problem (1.24), it follows that the rank of the system (1.25)-(1.26) is $r = |\gamma^\rho| + |\gamma^c| - (|\gamma^\rho_{ex}| + |\gamma^c_{ex}|) = |\gamma^\rho_{in}| + |\gamma^c_{in}|$. ☐

3.3 Proof of the Theorem 1.4 in Section 1.3

Let us first introduce new variables $\bar{\rho}^s := \sum_{l\in\gamma^\rho} R^\rho_{lp}\bar{\rho}^\gamma_l + f^{\bar{\rho}}_p - \bar{\rho}^\gamma_p$ and $c^s := f^c_p + \sum_{l\in\gamma^c} C^c_{lp}c^\gamma_l - c^\gamma_p$ Now, let us notice that from the definition of the new variables $\bar{\rho}^s$ and c^s, the definition of Difference Potential $P\mathbf{v}_\gamma = (P\bar{\rho}^\gamma, Pc^\gamma)$, and the definition of the vector function $\mathbf{f}$ (see Section 1.3), we have that $\bar{\rho}^s$ and c^s satisfy the following system of equations on sets $(M^1\backslash M^\rho)\cup\gamma^1$ and $(M^1\backslash M^c)\cup\gamma^1$ respectively:

$$\begin{aligned} \Delta_p\bar{\rho}^s - m\bar{\rho}^s_p &= 0, \quad p := (x_j, y_k) \in M^1\backslash M^\rho, &(3.5)\\ \bar{\rho}^s_p &= 0, \quad p \in \gamma^1 &(3.6)\end{aligned}$$

and,

$$\begin{aligned} \Delta_p c^s - mc^s_p &= 0, \quad p := (x_j, y_k) \in M^1\backslash M^c, &(3.7)\\ c^s_p &= 0, \quad p \in \gamma^1 &(3.8)\end{aligned}$$

Also, let us now assume that the conditions (1.27)-(1.28) are satisfied and let us notice that they can be rewritten in the new variables as:

$$\bar{\rho^s}_p = 0, \quad \text{for any point } p \in \gamma^\rho_{in} \tag{3.9}$$

$$c^s{}_p = 0, \quad \text{for any point } p \in \gamma^c_{in}. \tag{3.10}$$

Next, the sets γ^1 and γ^ρ_{in} can be considered as the boundary sets for the set $M^1\backslash M^\rho$. Similarly, the sets γ^1 and γ^c_{in} are the boundary sets for the set $M^1\backslash M^c$. Hence, from the equation (3.5) subject to the boundary conditions (3.9), (3.6), and the equation (3.7) subject to the boundary conditions (3.10) and (3.8), we have that:

$$\bar{\rho^s}_p = 0, \quad \forall p \in M^1\backslash M^\rho$$

and

$$c^s{}_p = 0, \quad \forall p \in M^1 \backslash M^c.$$

Since $\gamma^{\rho}_{ex} \subset M^1 \backslash M^{\rho}$ and $\gamma^{c}_{ex} \subset M^1 \backslash M^c$, we conclude that

$$\bar{\rho^s}_p = 0, \quad \forall p \in \gamma^{\rho}_{ex} \tag{3.11}$$

and

$$c^s{}_p = 0, \quad \forall p \in \gamma^{c}_{ex}. \tag{3.12}$$

Finally, let us notice that the system (1.25) - (1.26) can be rewritten in new variables $\bar{\rho^s}, c^s$ as:

$$\bar{\rho^s}_p = 0, \qquad \text{for any point } p \in \gamma^{\rho}_{in} \cup \gamma^{\rho}_{ex} \tag{3.13}$$

$$c^s{}_p = 0, \qquad \text{for any point } p \in \gamma^{c}_{in} \cup \gamma^{c}_{ex}. \tag{3.14}$$

Therefore, the system of the equations (3.9) - (3.10) implies the system (3.11)-(3.12), and hence the system (3.13) - (3.14). Finally, we know from Lemma 1.3 in Section 1.3 that the rank of the system (3.13) - (3.14) is $|\gamma^{\rho}_{in}| + |\gamma^{c}_{in}|$. Hence, the system (3.9) - (3.10) consists of the linearly independent equations. This concludes the proof. ☐

4 Concluding Remarks

We proposed a novel and efficient upwind-difference potentials scheme for chemotaxis models and closely related problems in physics and biology. The scheme can handle complex computational domains with the use of only Cartesian grids, and can be easily employed with fast Poisson solvers. The proposed method combines the simplicity of positivity-preserving upwind scheme on Cartesian meshes with the flexibility of the Difference Potentials method. Numerical experiments are presented to illustrate robustness of the upwind-difference potentials scheme.

Some of the future investigation includes the design of the adaptive strategy for the proposed method, the development of the domain decomposition procedure, and the extension of the scheme to other problems in physics and biology (see for example [43], [8, 9]).

Acknowledgment: The author is grateful to Viktor Ryaben'kii for his helpful discussion. The research is supported in part by the National Science Foundation Grant # DMS-1112984.

References

[1] J. Adler. Chemotaxis in bacteria. *Ann. Rev. Biochem.*, 44:341–356, 1975.

[2] J.T. Bonner. *The cellular slime molds.* Princeton University Press, Princeton, New Jersey, 2nd edition, 1967.

[3] Steve Bryson, Yekaterina Epshteyn, Alexander Kurganov, and Guergana Petrova. Well-balanced positivity preserving central-upwind scheme on triangular grids for the Saint-Venant system. *ESAIM Math. Model. Numer. Anal.*, 45(3):423–446, 2011.

[4] E.O. Budrene and H.C. Berg. Complex patterns formed by motile cells of escherichia coli. *Nature*, 349:630–633, 1991.

[5] E.O. Budrene and H.C. Berg. Dynamics of formation of symmetrical patterns by chemotactic bacteria. *Nature*, 376:49–53, 1995.

[6] Thierry Buffard and Stphane Clain. Monoslope and multislope muscl methods for unstructured meshes. *Journal of Computational Physics*, 229(10):3745 – 3776, 2010.

[7] Caterina Calgaro, Emile Chane-Kane, Emmanuel Creusé, and Thierry Goudon. L^∞-stability of vertex-based MUSCL finite volume schemes on unstructured grids: simulation of incompressible flows with high density ratios. *J. Comput. Phys.*, 229(17):6027–6046, 2010.

[8] Claire Chainais-Hillairet and Francis Filbet. Asymptotic behaviour of a finite-volume scheme for the transient drift-diffusion model. *IMA J. Numer. Anal.*, 27(4):689–716, 2007.

[9] Claire Chainais-Hillairet, Jian-Guo Liu, and Yue-Jun Peng. Finite volume scheme for multidimensional drift-diffusion equations and convergence analysis. *M2AN Math. Model. Numer. Anal.*, 37(2):319–338, 2003.

[10] A. Chertock, Y. Epshteyn, and A. Kurganov. High-order finite-difference and finite-volume methods for chemotaxis models. 2010. in preparation.

[11] A. Chertock and A. Kurganov. A positivity preserving central-upwind scheme for chemotaxis and haptotaxis models. *Numer. Math.*, 111:169–205, 2008.

[12] S. Childress and J.K. Percus. Nonlinear aspects of chemotaxis. *Math. Biosc.*, 56:217–237, 1981.

[13] Ivan Christov and Bojan Popov. New non-oscillatory central schemes on unstructured triangulations for hyperbolic systems of conservation laws. *J. Comput. Phys.*, 227(11):5736–5757, 2008.

[14] M.H. Cohen and A. Robertson. Wave propagation in the early stages of aggregation of cellular slime molds. *J. Theor. Biol.*, 31:101–118, 1971.

[15] Yves Coudière, Thierry Gallouët, and Raphaèle Herbin. Discrete Sobolev inequalities and L^p error estimates for finite volume solutions of convection diffusion equations. *M2AN Math. Model. Numer. Anal.*, 35(4):767–778, 2001.

[16] Yves Coudière, Jean-Paul Vila, and Philippe Villedieu. Convergence rate of a finite volume scheme for a two-dimensional convection-diffusion problem. *M2AN Math. Model. Numer. Anal.*, 33(3):493–516, 1999.

[17] Komla Domelevo and Pascal Omnes. A finite volume method for the Laplace equation on almost arbitrary two-dimensional grids. *M2AN Math. Model. Numer. Anal.*, 39(6):1203–1249, 2005.

[18] Yekaterina Epshteyn. Discontinuous Galerkin methods for the chemotaxis and haptotaxis models. *J. Comput. Appl. Math.*, 224(1):168–181, 2009.

[19] Yekaterina Epshteyn and Ahmet Izmirlioglu. Fully discrete analysis of a discontinuous finite element method for the Keller-Segel chemotaxis model. *J. Sci. Comput.*, 40(1-3):211–256, 2009.

[20] Yekaterina Epshteyn and Alexander Kurganov. New interior penalty discontinuous Galerkin methods for the Keller-Segel chemotaxis model. *SIAM J. Numer. Anal.*, 47(1):386–408, 2008/09.

[21] F. Filbet. A finite volume scheme for the patlak-keller-segel chemotaxis model. *Numer. Math.*, 104:457–488, 2006.

[22] Jan Haškovec and Christian Schmeiser. Stochastic particle approximation for measure valued solutions of the 2D Keller-Segel system. *J. Stat. Phys.*, 135(1):133–151, 2009.

[23] Miguel A. Herrero and Juan J. L. Velázquez. A blow-up mechanism for a chemotaxis model. *Ann. Scuola Norm. Sup. Pisa Cl. Sci. (4)*, 24(4):633–683 (1998), 1997.

[24] D. Horstmann. From 1970 until now: The keller-segel model in chemotaxis and its consequences i. *Jahresber. DMV*, 105:103–165, 2003.

[25] D. Horstmann. From 1970 until now: The keller-segel model in chemotaxis and its consequences ii. *Jahresber. DMV*, 106:51–69, 2004.

[26] Willem Hundsdorfer and Jan Verwer. *Numerical solution of time-dependent advection-diffusion-reaction equations*, volume 33 of *Springer Series in Computational Mathematics*. Springer-Verlag, Berlin, 2003.

[27] E.F. Keller and L.A. Segel. Initiation of slime mold aggregation viewed as an instability. *J. Theor. Biol.*, 26:399–415, 1970.

[28] E.F. Keller and L.A. Segel. Model for chemotaxis. *J. Theor. Biol.*, 30:225–234, 1971.

[29] E.F. Keller and L.A. Segel. Traveling bands of chemotactic bacteria: A theoretical analysis. *J. Theor. Biol.*, 30:235–248, 1971.

[30] Alexander Kurganov and Guergana Petrova. A second-order well-balanced positivity preserving central-upwind scheme for the Saint-Venant system. *COMMUNICATIONS IN MATHEMATICAL SCIENCES*, 5(1):133–160, MAR 2007.

[31] Alexander Kurganov and Eitan Tadmor. New high-resolution central schemes for nonlinear conservation laws and convection-diffusion equations. *J. Comput. Phys.*, 160(1):241–282, 2000.

[32] A. Marrocco. 2d simulation of chemotaxis bacteria aggregation. *M2AN Math. Model. Numer. Anal.*, 37:617–630, 2003.

[33] Orhan Mehmetoglu and Bojan Popov. Maximum principle and convergence of central schemes based on slope limiters. *Math. Comp.*, 81(277):219–231, 2012.

[34] V. Nanjundiah. Chemotaxis, signal relaying and aggregation morphology. *J. Theor. Biol.*, 42:63–105, 1973.

[35] Haim Nessyahu and Eitan Tadmor. Nonoscillatory central differencing for hyperbolic conservation laws. *J. Comput. Phys.*, 87(2):408–463, 1990.

[36] C.S. Patlak. Random walk with persistence and external bias. *Bull. Math: Biophys.*, 15:311–338, 1953.

[37] Benoît Perthame. *Transport equations in biology.* Frontiers in Mathematics. Birkhäuser Verlag, Basel, 2007.

[38] L.M. Prescott, J.P. Harley, and D.A. Klein. *Microbiology.* Wm. C. Brown Publishers, Chicago, London, 3rd edition, 1996.

[39] V. S. Ryaben′kiĭ, V. I. Turchaninov, and E. Yu. Èpshteĭn. An algorithm composition scheme for problems in composite domains based on the method of difference potentials. *Zh. Vychisl. Mat. Mat. Fiz.*, 46(10):1853–1870, 2006.

[40] V.S. Ryaben'kii. Method of difference potentials and its applications. *Springer-Verlag*, 2001.

[41] Norikazu Saito. Conservative upwind finite-element method for a simplified Keller-Segel system modelling chemotaxis. *IMA J. Numer. Anal.*, 27(2):332–365, 2007.

[42] R. Strehl, A. Sokolov, D. Kuzmin, and S. Turek. A flux-corrected finite element method for chemotaxis problems. *Computational Methods in Applied Mathematics*, 10(2):219–232, 2010.

[43] Idan Tuval, Luis Cisneros, Christopher Dombrowski, Charles W. Wolgemuth, John O. Kessler, and Raymond E. Goldstein. Bacterial swimming and oxygen transport near contact lines. *PNAS*, 102 (7):2277–2282, 2005.

[44] R. Tyson, S.R. Lubkin, and J.D. Murray. A minimal mechanism for bacterial pattern formation. *Proc. Roy. Soc. Lond. B*, 266:299–304, 1999.

[45] R. Tyson, L.G. Stern, and R.J. LeVeque. Fractional step methods applied to a chemotaxis model. *J. Math. Biol.*, 41:455–475, 2000.